

AD-A048 045

SIGNETICS CORP SUNNYVALE CALIF
CANTILEVER ACCELEROMETER.(U)
SEP 77 W C ROSVOLD, M L STEPHENS

F/G 14/2

UNCLASSIFIED

AFAL-TR-77-152

F33615-76-C-1159
NL

1 OF 1
AD
A048045



AD-A048045

AFAL-TR-77-152

1



CANTILEVER ACCELEROMETER

Signetics Corporation
811 East Arques Avenue
P. O. Box 9052
Sunnyvale, California 94086

SEPTEMBER 1977

Technical Report AFAL-TR-77-152

Final Report

March 1976 - January 1977

Distribution limited to U. S. Government agencies only; report contains sensitive test data August 1977. Other requests for this report should be directed to AFAL/TWA, Wright-Patterson AFB, Ohio 45433.

Approved for Public Release, Distribution Unlimited.

ORIGINAL CONTAINS COLOR PLATES: ALL DDC REPRODUCTIONS WILL BE IN BLACK AND WHITE.

AIR FORCE AVIONICS LABORATORY
AIR FORCE WRIGHT AERONAUTICAL LABORATORIES
AIR FORCE SYSTEMS COMMAND
WRIGHT-PATTERSON AIR FORCE BASE, OHIO 45433

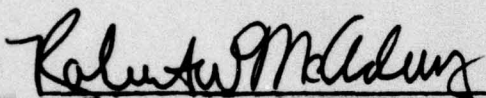
DDC
RECEIVED
JAN 5 1978
REGULATED
D

NOTICE

When Government drawings, specifications, or other data are used for any purpose other than in connection with a definitely related Government procurement operation, the United States Government thereby incurs no responsibility nor any obligation whatsoever; and the fact that the government may have formulated, furnished, or in any way supplied the said drawings, specifications, or other data, is not to be regarded by implication or otherwise as in any manner licensing the holder or any other person or corporation, or conveying any rights or permission to manufacture, use, or sell any patented invention that may in any way be related thereto.

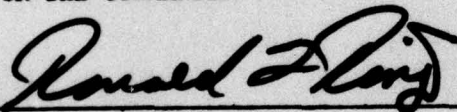
This report has been reviewed by the Information Office (OI) and is releasable to the National Technical Information Service (NTIS). At NTIS, it will be available to the general public, including foreign nations.

This technical report has been reviewed and is approved for publication.



ROBERT W. MCADORY, Project Engineer
Reference Systems Technology Group
Reference Systems Branch, Reconnaissance
and Weapon Delivery Division

FOR THE COMMANDER



RONALD L. RINGO
Chief, Reference Systems Branch
Reconnaissance and Weapon Delivery Div.

"If your address has changed, if you wish to be removed from our mailing list, or if the addressee is no longer employed by your organization please notify AFAL/RWA, W-PAFB, OH 45433 to help us maintain a current mailing list".

Copies of this report should not be returned unless return is required by security considerations, contractual obligations, or notice on a specific document.

REPORT DOCUMENTATION PAGE		READ INSTRUCTIONS BEFORE COMPLETING FORM
1. REPORT NUMBER AFAL-TR-77-152	2. GOVT ACCESSION NO.	3. RECIPIENT'S CATALOG NUMBER
4. TITLE (and Subtitle) CANTILEVER ACCELEROMETER		5. TYPE OF REPORT & PERIOD COVERED Final July 1975 to August 1977
		6. PERFORMING ORG. REPORT NUMBER
7. AUTHOR(s) Warren C. Rosvold, Mark L. Stephens		8. CONTRACT OR GRANT NUMBER(s) F33615-76-C-1159
9. PERFORMING ORGANIZATION NAME AND ADDRESS . Signetics Sunnyvale CA 94086		10. PROGRAM ELEMENT, PROJECT, TASK AREA & WORK UNIT NUMBERS P.E. 62204F Project 6095 1201
11. CONTROLLING OFFICE NAME AND ADDRESS Air Force Avionics Laboratory/RWA Wright-Patterson AFB OH 45433		12. REPORT DATE September 1977
		13. NUMBER OF PAGES 79
14. MONITORING AGENCY NAME & ADDRESS (if different from Controlling Office)		15. SECURITY CLASS. (of this report) Unclassified
		15a. DECLASSIFICATION/DOWNGRADING SCHEDULE
16. DISTRIBUTION STATEMENT (of this Report) Approved for Public Release, Distribution Unlimited.		
17. DISTRIBUTION STATEMENT (of the abstract entered in Block 20, if different from Report)		
18. SUPPLEMENTARY NOTES		
19. KEY WORDS (Continue on reverse side if necessary and identify by block number) Accelerometer, open loop accelerometer, integrated circuit fabrication, silicon accelerometer, low cost accelerometer		
20. ABSTRACT (Continue on reverse side if necessary and identify by block number) Four accelerometer models were designed, manufactured and evaluated during the term of the contract. These were built using single crystalline silicon and integrated circuit fabrication techniques. The basic physical structure used on all accelerometer models was the "H" geometry. The difference between the models was the topographical locations of the piezoresistor bridge, and electronic components which were adjusted in order to obtain optimized accelerometer performance.		

ACCESSION for	
NTIS	White Section <input checked="" type="checkbox"/>
DDC	Buff Section <input type="checkbox"/>
UNANNOUNCED	<input type="checkbox"/>
JUSTIFICATION	
BY	
DISTRIBUTION/AVAILABILITY CODES	
Dist.	AVAIL. 2nd/3rd SPECIAL
A	

PREFACE

Signetics has produced a silicon semiconductor transducer, based on the proprietary (patent applied for) superlinear folded cantilever, beam spring design jointly developed by Signetics and DiAx Corporation, with preliminary work performed for the Air Force as a subcontractor to DiAx.

By use of anisotropic etching techniques, the silicon is shaped into the folded cantilever spring with a thick supporting structure of silicon surrounding the spring. The anisotropic etch technique is an etching technique which is sensitive to the different crystal planes of the silicon. Since the etching follows the crystal planes, very accurate control of the size of the slots, and the thickness of the spring member is possible.

Four piezoresistive elements are ion implanted at high stress regions on the spring structure. Two are oriented so that their resistance increases with acceleration, and two are oriented so that it decreases. When connected in a bridge configuration, any acceleration unbalances the bridge and creates a signal that is proportional to the acceleration force.

Advanced integrated circuit processing techniques are used to produce these devices and many devices are simultaneously batch processed on a single three inch diameter silicon wafer. Therefore, the fabrication of this sensor will utilize the advantages of small size, mass production, and low production costs inherent in solid state devices to manufacture this accelerometer.

The Department of Aeronautics at Stanford University conducted the dynamic evaluation of the accelerometer with regard to linearity, frequency response, and range.

TABLE OF CONTENTS

SECTION		PAGE
I	INTRODUCTION	1
II	MK I ACCELEROMETER	3
III	ION IMPLANTATION	9
IV	PACKAGING	16
V	MK II ACCELEROMETER	24
VI	MK III PROTOTYPE ACCELEROMETER	37
VII	MK III ACCELEROMETER	44
	APPENDIX	69

LIST OF FIGURES

<u>Figure</u>		<u>Page</u>
<u>MK I ACCELEROMETER/SECTION 2</u>		
1	Mk I in Package	4
2	Mk I Layout	5
3	Mk I Output ± 1 g	7
<u>ION IMPLANTED PIEZORESISTORS/SECTION 3</u>		
4	Implant vs. Diffused Resistor T. C. Comparison	10
5	Anneal Time 15 min T. C. Curve	12
6	Anneal Time 30 min T. C. Curve	13
7	Anneal Time 60 min T. C. Curve	14
8	Anneal Time 90 min T. C. Curve	15
<u>ACCELEROMETER PACKAGING/SECTION 4</u>		
9	Interface Chip Packaging	17
10	Interface Chip Metallurgy	18
11	Accelerometer Metallurgy	18
12	Accelerometer Assembly Drawing	19
13	Mk III Assembly Photo	20
14	Argon Damping	23
15	Nitrogen Damping	23
16	Evacuated Chamber Damping	23
<u>MK II ACCELEROMETER/SECTION 5</u>		
17	Mk II Accelerometer Photo	25
18	Mk II Interface Chip Package Assembly	26
19	Mk II Accelerometer Layout	28
20	Dynamic Testing Apparatus	30
21	Accelerometer Output	31
22	Accelerometer Linearity Curve	32
23	Frequency Response at 1 g	33
24	Frequency Response at 1 g Curve	34
<u>MK III PROTOTYPE ACCELEROMETER/SECTION 6</u>		
25	Mk III Prototype Photo	38
26	Mk III Prototype in Package	39
27	Mk II Resistor Membrane Geometry	40
28	Mk III Resistor Membrane Geometry	40
29	Mk III Prototype Accelerometer Layout	41
30	Mk III Prototype ± 1 g Linearity Curve	43

LIST OF FIGURES (continued)

<u>Figure</u>	<u>MK III ACCELEROMETER/SECTION 7</u>	<u>Page</u>
31	Mk III Accelerometer	45
32	Mk III Accelerometer/Interface Chip Assembly	46
33	Mk II Resistor/Membrane Geometry	49
34	Mk III Resistor/Membrane Geometry	49
35	Mk III Layout	50
36	Mk III Accelerometer Cell	51
37	Mk III Schematic	52
38	Piezoresistor/Temp. Control Active Region	53
39	Resistor Test Structures	54
40	Transistor Test Structures	55
41	Probing Bonding Pad	56
42	Depth Gauges - Front Side	57
43	Depth Gauges - Back Side	58
44	Mk III Testing at Signetics - Summary	60
45	Mk III Testing at Stanford Zero Phase/Bias Determination	65
46	Mk III Testing at Stanford $\pm 1g$ Leitz Head Output (1)	66
47	Mk III Testing at Stanford $\pm 1g$ Leitz Head Output (2)	67

SECTION I
INTRODUCTION

During the contract period four accelerometer designs were evaluated.

- 1) Mk I, Double Ended, Orthogonal Resistors
- 2) Mk II, Double Ended Orthogonal Resistors with Dual Temp Control Circuitry
- 3) Mk III, Prototype, Single Ended, Unidirectional Resistors
- 4) Mk III, Single Ended, Unidirectional Resistors with Quad Temp Control Circuitry

These designs differed in that the topographical locations of the resistor bridge and electronic components with respect to the membrane's physical geometry were altered in order to obtain optimized accelerometer performance. In the prototype designs no temp. control circuitry was included because only the optimization of the resistor orientation and location was to be determined.

This results in a batch processed microelectronic accelerometer having the following advantages:

- 1) Small size/mass,
- 2) Low cost,
- 3) Zero hysteresis,
- 4) High reliability.

The general description of the accelerometer structure is as follows: Using anisotropic etching techniques, the silicon is shaped into the folded cantilever spring with a thick supporting structure of silicon surrounding the spring. The anisotropic etch technique is an etching technique which is sensitive to the different crystal planes of the silicon. Since the etching follows the crystal planes, very accurate control of the size of the slots, and the thickness of the spring member is possible.

Four piezoresistive elements are implanted at high stress regions on the spring structure. Two are oriented so that their resistance increases with acceleration, and two are oriented so that it decreases. When connected in a bridge configuration, any acceleration unbalances the bridge and creates a signal that is proportional to the acceleration force.

Advanced integrated circuit processing techniques are used to produce these devices and many devices are simultaneously batch processed on a single three inch diameter silicon wafer.

The overall dimensions of the accelerometer chip for all four designs are 0.174 in. wide, 0.245 in. long by 0.007 in. at the thickest point. The piezoresistive membrane is typically 0.001 in. thick.

These four accelerometer designs and associated technology are presented in Sections 2 - 7 together with illustrations and in-depth dialogue.

The general format of the four accelerometer sections is as follows:

- 1) Photos of the Accelerometer,
- 2) Design,
- 3) Accelerometer Layout,
- 4) Testing Results,
- 5) Critique and Recommendations.

SECTION II

MK I ACCELEROMETER

The Mk I transducer design evolved from a critical analysis of the Mk Ø prototype. The basic problems with the Mk Ø were low sensitivity and a very large temperature coefficient. We felt that these problems were due to the large separation between piezoresistors (nearly 50 mils on the Mk Ø) and the fact that the piezoresistors were not in a region of maximum stress.

The Mk I design changed the location of the piezoresistors to the ends of the membrane, as shown in Figure 2. They were previously located (in the Mk Ø) in the four areas bounded by dotted lines in Figure 2. By bringing the resistors closer together, we expected better matching and lower differential temperature coefficients. By placing the resistors where we did, we expected greater sensitivity, since the end of the membrane had been theoretically shown to be the region of maximum stress in the membrane structure.

Two additional features were incorporated into the Mk I. The Mk Ø used a continuous resistor structure which reduced the sensitivity due to the "bends" of the resistor. To correct this, all resistor elements were made parallel and metal was used in place of silicon to connect the sub-pieces. Also, the Mk Ø had metal runs going over the piezoresistors which caused breakdown problems. In the Mk I all metal was removed from the piezoresistor area, except for the direct interconnect to the contacts.

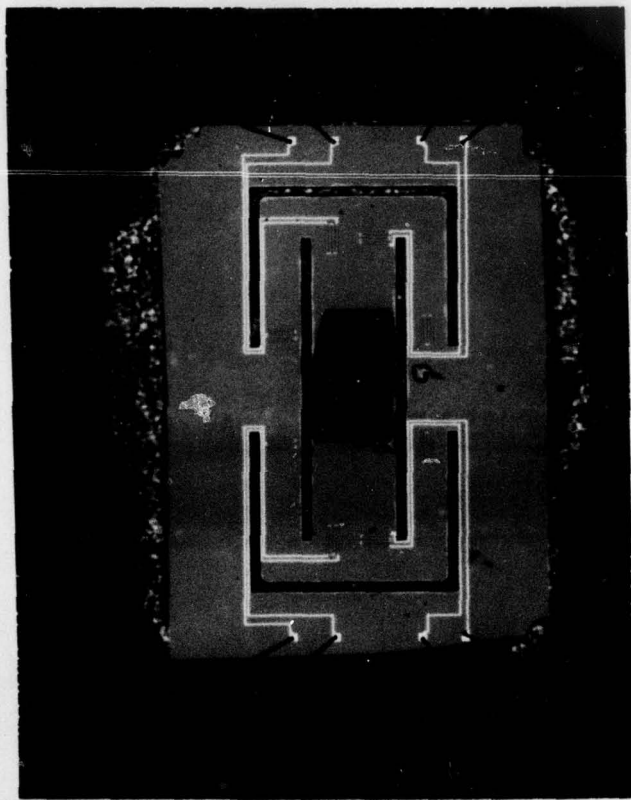
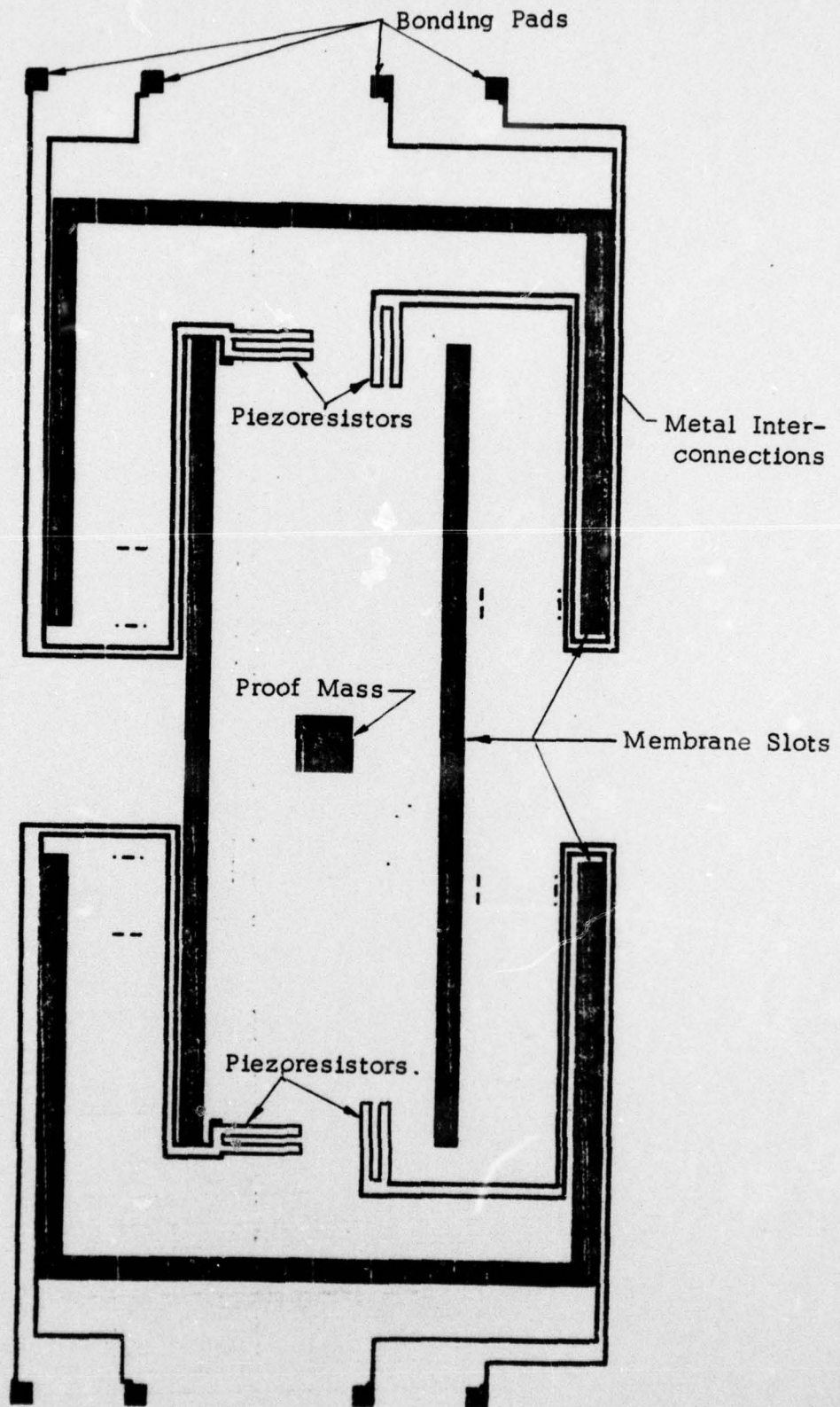


Fig. 1
Mk I Accelerometer



Mk I Accelerometer Layout

Fig. 2

TEST RESULTS

The sensitivity of the Mk I was nearly double the sensitivity of the Mk 0. In addition it showed a static non-linearity of .1% of full scale. The sinusoidal curve in Figure 3 shows relative output as the device was rotated through 360° on an indexing head. The larger noise curve represents the total non-linearity of the device when fixed offsets and temperature drift were mathematically removed from the data. Observe that it has a $\cos 2\theta$ dependence, indicating a second order non-linearity is operating. The smaller noise curve represents the residual noise of the device when all non-linear components have been removed.

The fundamental noise limit is due to excess noise (1/f frequency spectrum) in the piezoresistors. This type of noise source is common in solid state devices and is related to surface conditions in the Si/SiO₂ interface. Generally, it can be reduced by improving the overall cleanliness of the process and preventing ionic contaminants from reaching the interface area. In addition there is some theoretical evidence that 1/f noise can be enhanced by local stress patterns in the silicon membrane. This theory will have to be evaluated in future tests with the accelerometer.

TRANSDUCER NON-LINEARITY VS ROTATION

t 1g

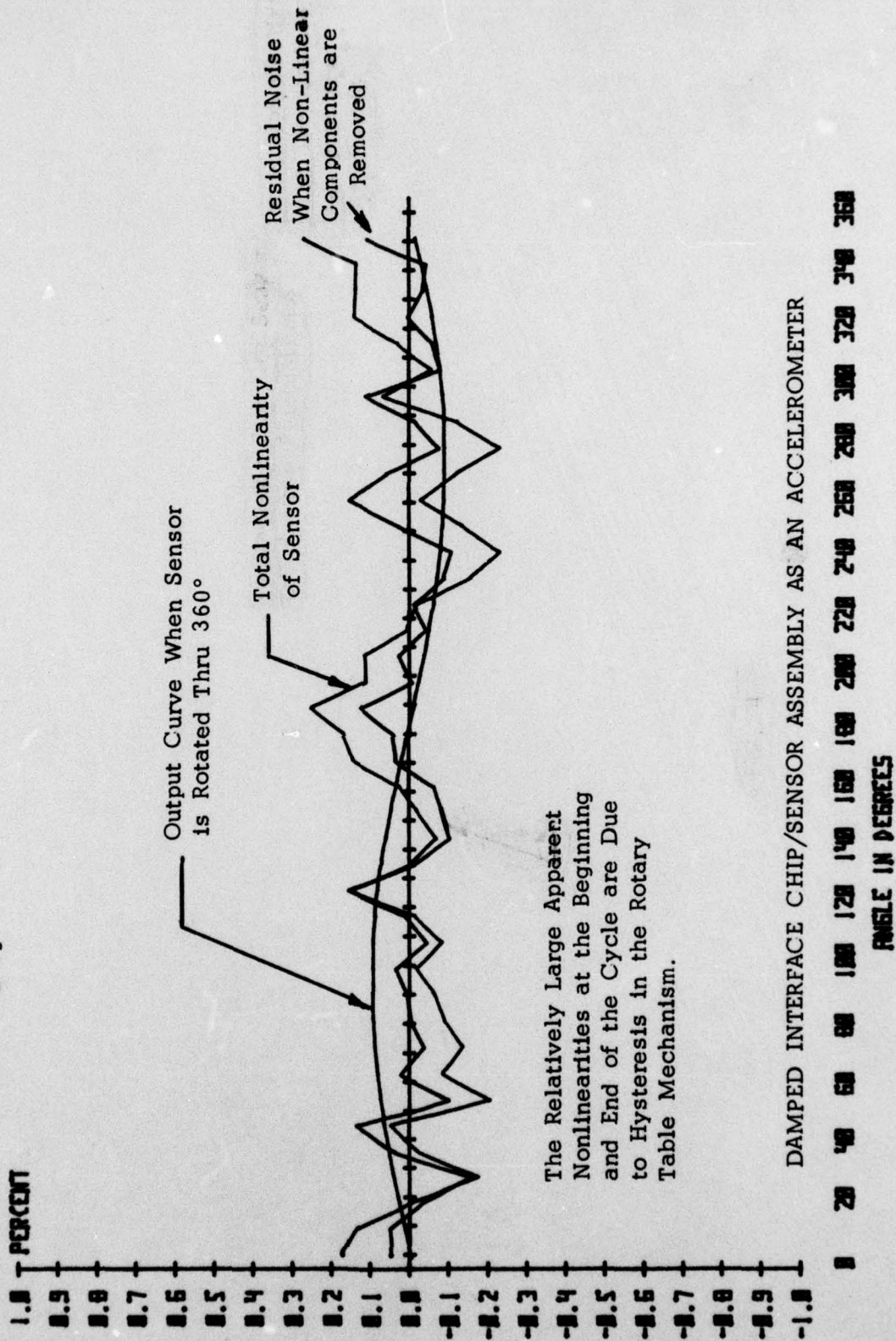


Fig. 3

CRITIQUE AND RECOMMENDATIONS

The Mk I accelerometer satisfied one of its design goals, to increase sensitivity of the device to acceleration. However, it failed to improve the temperature sensitivity problem. Large mismatches between bridge resistors still existed with associated large differential temperature coefficients.

An analysis of the probable causes of the temperature sensitivity problem showed that it was most likely due to statistical matching between the diffused piezoresistors, which have inherently large tempcos. We essentially felt that the matching was poor due to the fact that our basic piezoresistor (a diffused component) was highly sensitive to temperature and processing conditions. By making the basic resistor less sensitive to temperature and processing, we felt that we could then realize an improvement in matching over temperature.

To achieve our goal of a better basic piezoresistor we decided to redesign the Mk I accelerometer to incorporate "zero TC" ion implanted resistors. The piezoresistor width was also doubled to reduce matching errors due to photolithography. We felt that wider, ion implanted resistors would solve the temperature problem since we could

- a) reduce the basic tempco of the piezoresistor to zero around a specific operating temperature,
- b) match the resistors better due to the increased size and implantation method.

As an additional safeguard we incorporated a temperature control loop with dual heaters and sensors on the transducer die, to control the chip temperature. By this method we felt that we could control the die temperature to 1°C over the full military range. The temperature control system would reduce the requirements for matching of the piezoresistors, and improve the chances of success.

SECTION III

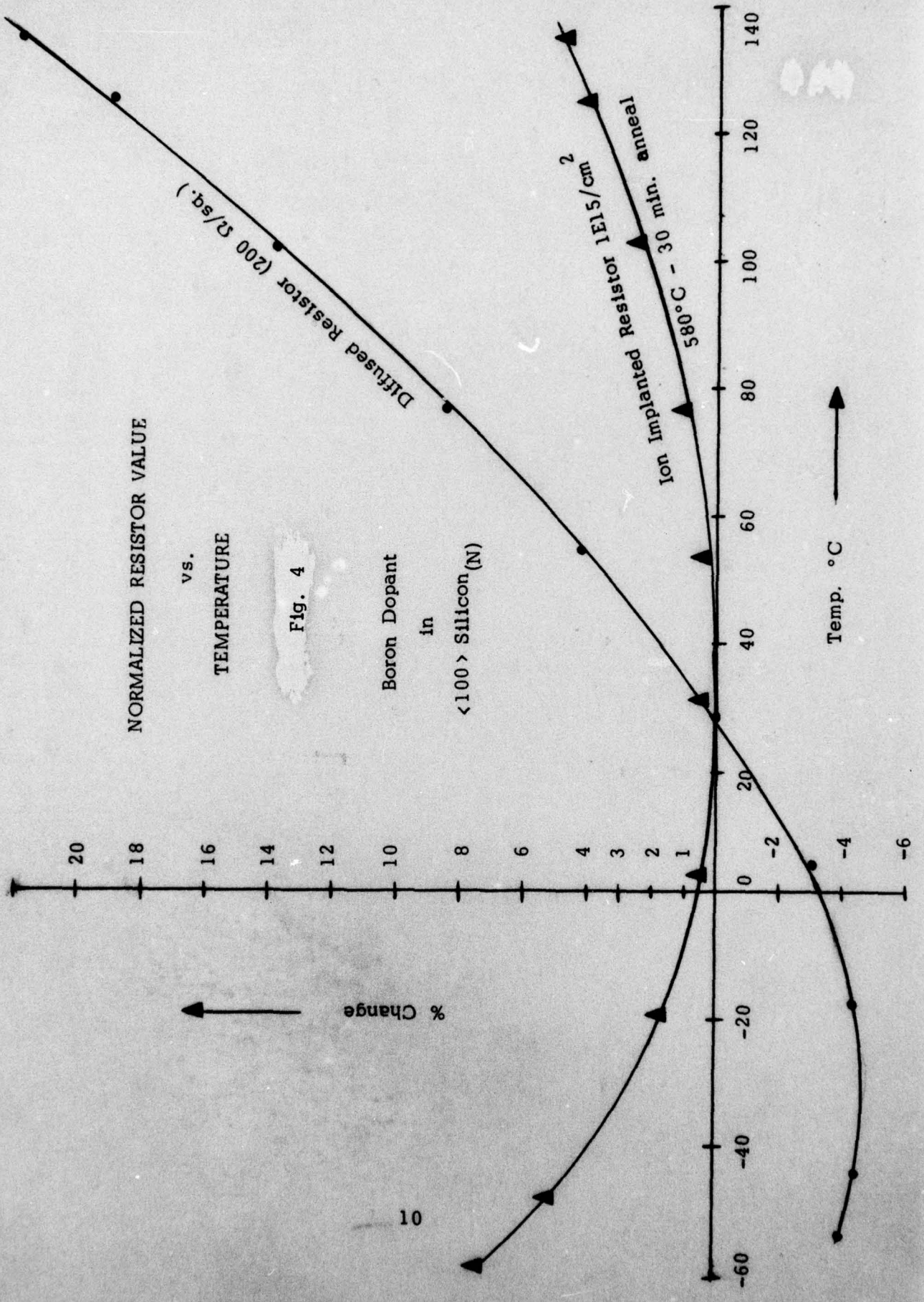
ION IMPLANTED PIEZORESISTOR BRIDGE

Ion implanted piezoresistor bridges were used in the fabrication of Mk II, Mk III prototype and Mk III accelerometers. We chose ion implantation as an obvious alternative to the more conventional thermal diffusion process because of dramatic superiorities in both temperature coefficient and range of sheet resistivities.

To determine a suitable resistor process for solid state accelerometers a comparative evaluation of resistors made by the standard-diffusion and ion implantation processes was carried out. The experiment was done with production processing, and a large number of devices were processed so that statistical analysis could be performed on the data.

Figure 4 shows the superior temperature coefficient of ion implanted resistors compared with thermally diffused resistors.

Since the ion dose can be controlled very accurately, excellent definition of the absolute value of resistors, as well as good matching between resistor pairs, can be obtained. Also, since the device, unlike a thin film resistor, is formed within the semiconductor substrate, it is passivated by silicon dioxide in the same manner as a diffused resistor. In other words the ion implanted resistor combines the advantages of bulk diffused devices with the high sheet resistance of thin film devices. The unique characteristics of ion implantation have been combined with standard bipolar process technology to achieve the high precision required by this accelerometer. Thus, the accelerometer can be manufactured on the same process line with ultrahigh volume circuits such as operational amplifiers with only a minimum of extra handling.



ION IMPLANTATION ANNEAL STUDY

The variation of ion implanted resistors with temperature is a strong function of the ion dosage, the anneal temperature and the anneal time. Annealing is required after implantation to activate the acceptor atoms in the silicon lattice.

For this initial study, we fixed the dosage at 10^{15} atoms/cm² and the anneal temperature at 580°C. We varied the anneal time from 15 minutes to 120 minutes. The effect is clear from the graphs. The short anneal times produce a good "zero-TC" resistor at elevated temperatures (good for temperature control at 100°C). The higher anneal times produce a good "zero-TC" resistor at lower temperatures near 25°C (good for non-temperature controlled applications). In general, the longer the anneal time, more curvature is produced in the resistance vs. temperature curve and it tends to be "rocked" counter-clockwise to produce a higher variation at elevated temperatures.

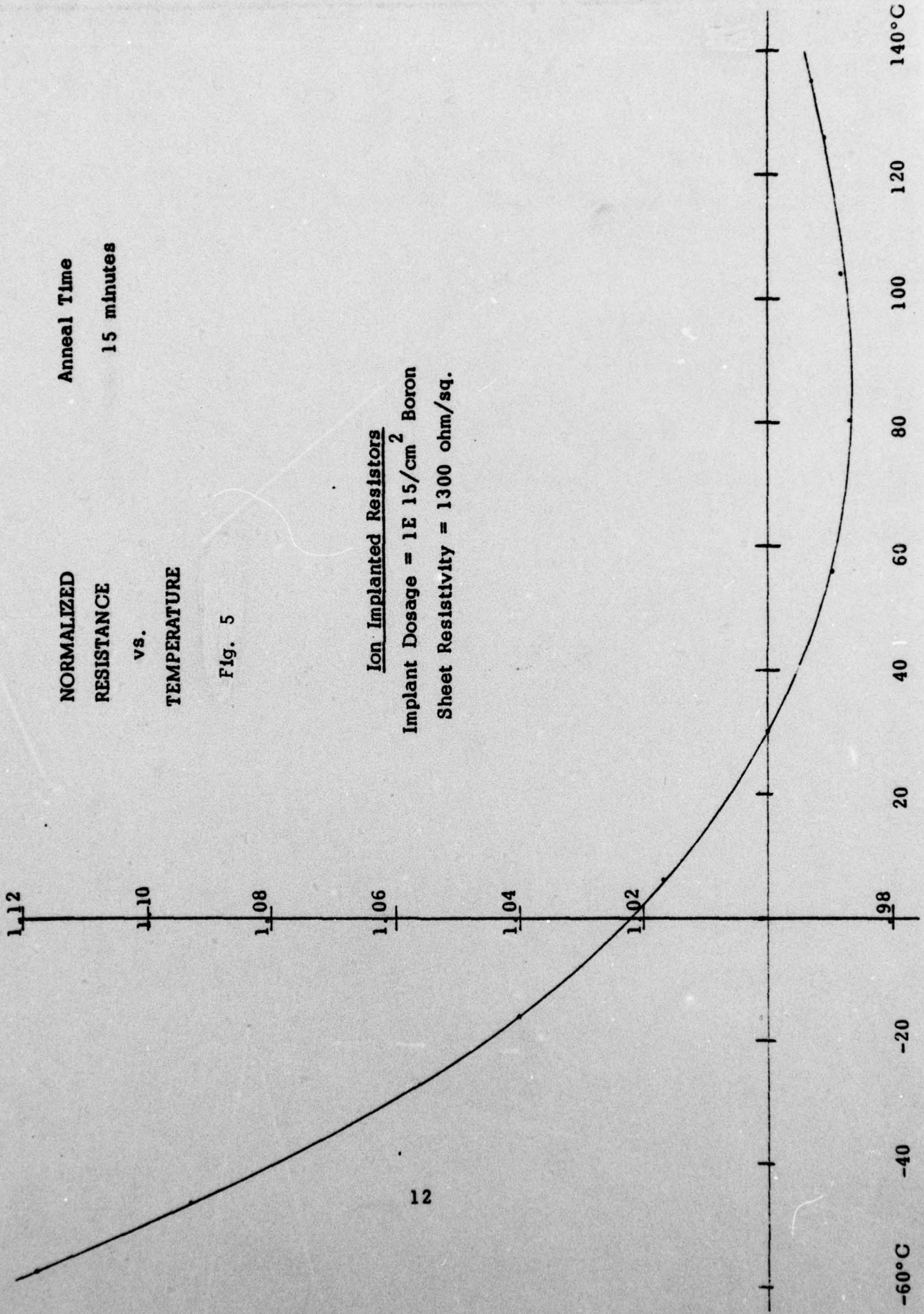
In performing the experimental work for this study, two problem areas were uncovered. First, there is a substantial variation in the resistance curves from die to die under the same anneal conditions. Second, roughly 50% of the tested die showed a dominant leakage current (resistor to tub) which caused measurement problems at temperatures over 120°C. Both of these problems would cause serious limitations for a piezoresistive sensor, since the first problem would destroy TC matching and the second would rule out temperature controlled operation at a reasonably high temperature. These will be studied in greater depth in the future.

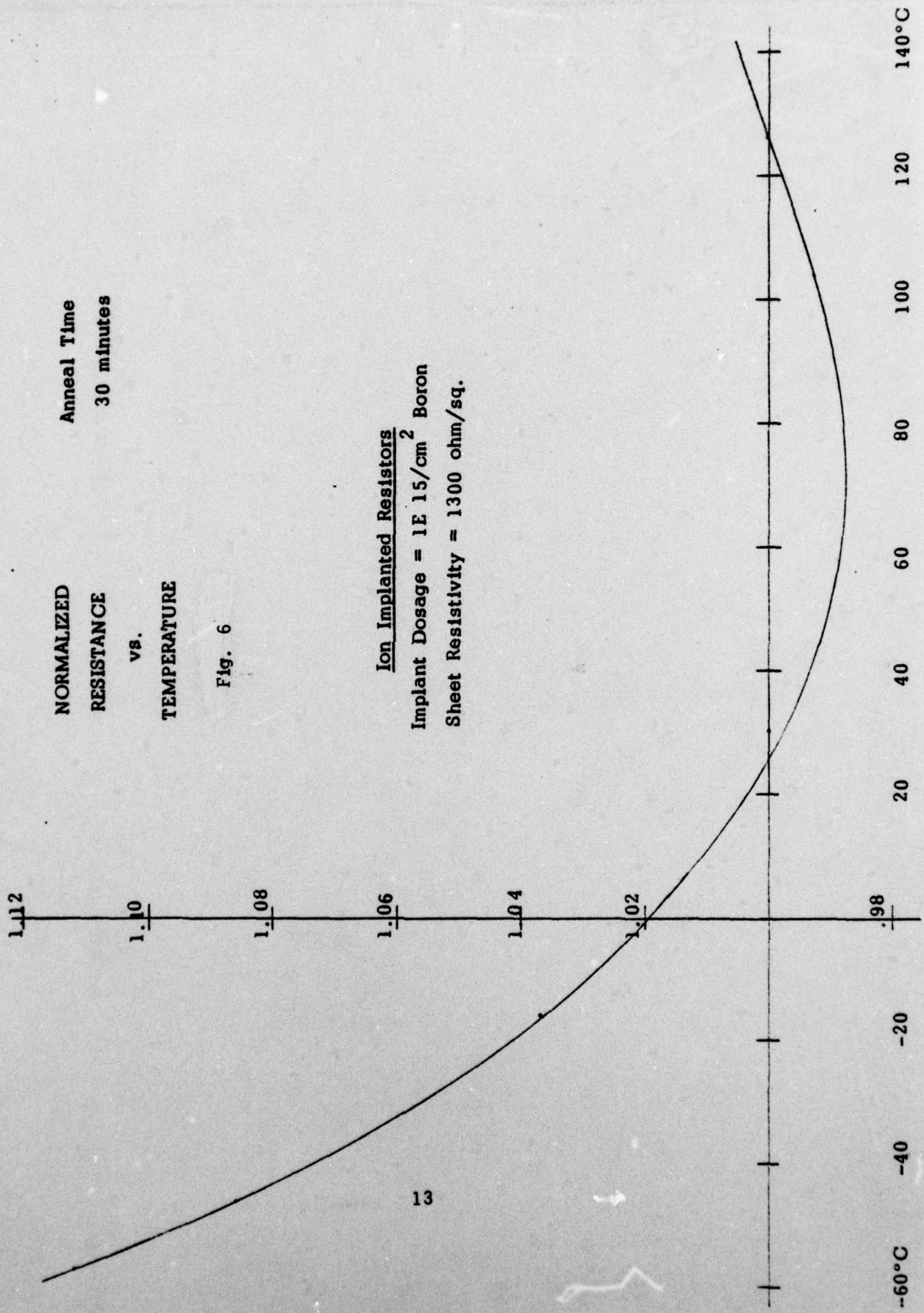
**NORMALIZED
RESISTANCE
vs.
TEMPERATURE**

**Anneal Time
15 minutes**

Fig. 5

Ion Implanted Resistors
Implant Dosage = $1 \text{E } 15/\text{cm}^2$ Boron
Sheet Resistivity = 1300 ohm/sq.





**NORMALIZED
RESISTANCE
vs.
TEMPERATURE**

**Anneal Time
30 minutes**

Fig. 6

Ion Implanted Resistors
Implant Dosage = $1E 15/cm^2$ Boron
Sheet Resistivity = 1300 ohm/sq.

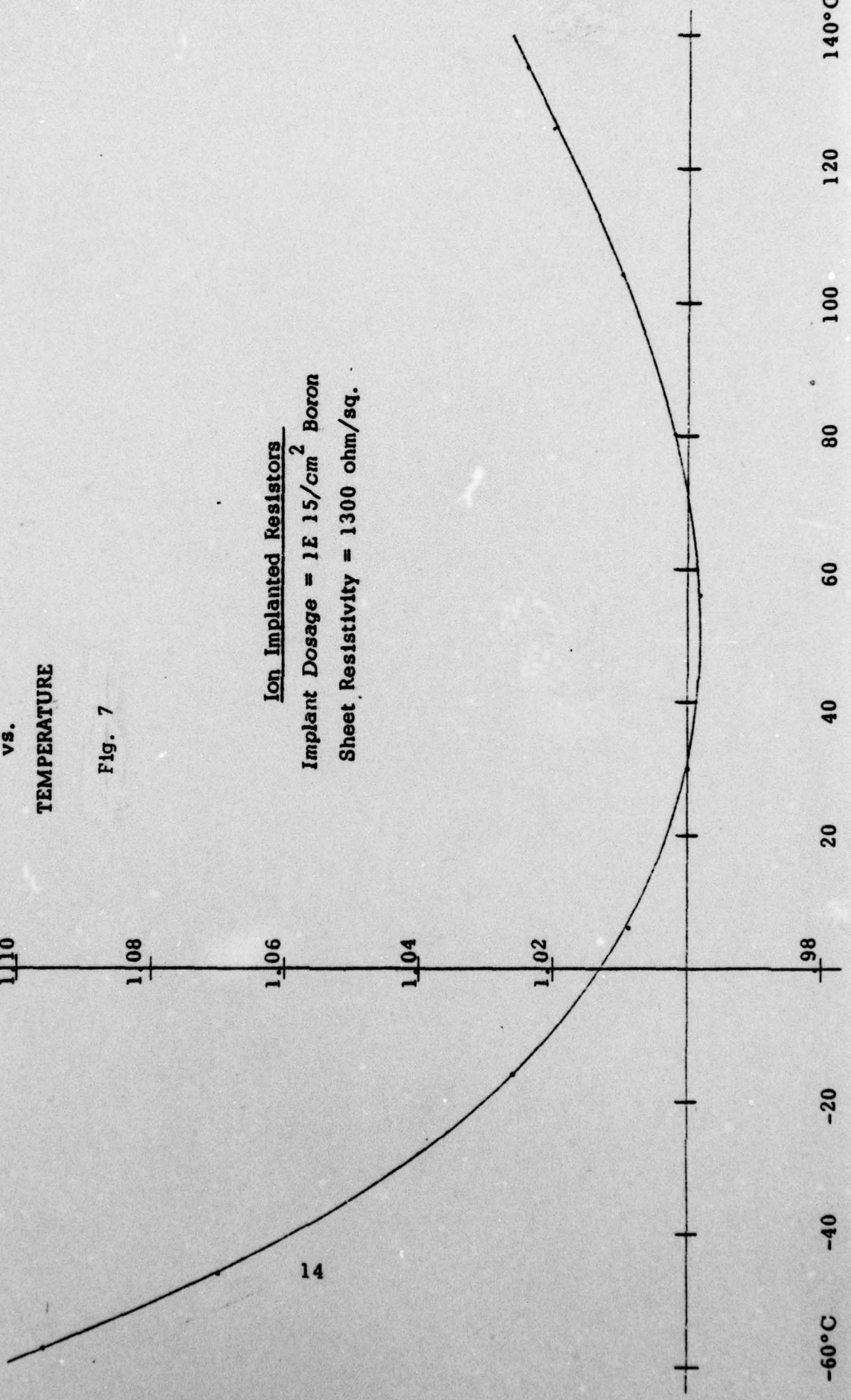
1.12
1.10
1.08
1.06
1.04
1.02
98

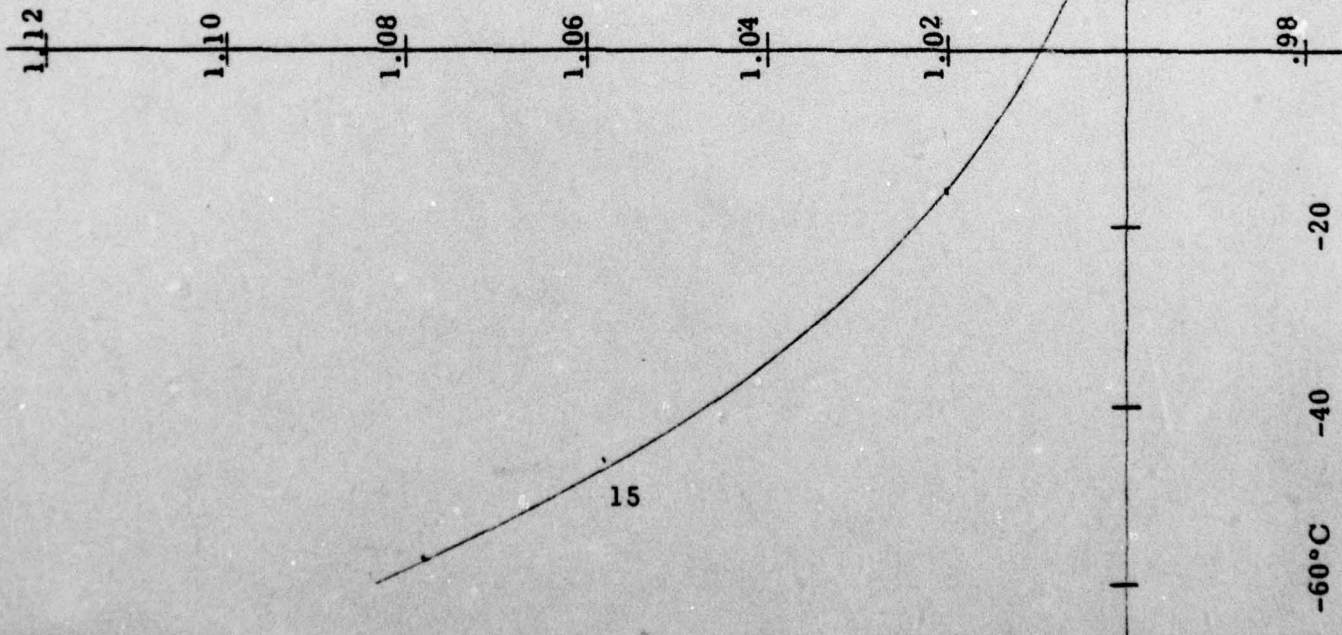
NORMALIZED
RESISTANCE
vs.
TEMPERATURE

Anneal Time
60 minutes

Fig. 7

Ion Implanted Resistors
Implant Dosage = $1E 15/cm^2$ Boron
Sheet Resistivity = 1300 ohm/sq.





**NORMALIZED
RESISTANCE
vs.
TEMPERATURE**

**Anneal Time
120 minutes**

Fig. 8

Ion Implanted Resistors
Implant Dosage = $1E 15/cm^2$ Boron
Sheet Resistivity = 1300 ohm/sq.

SECTION IV

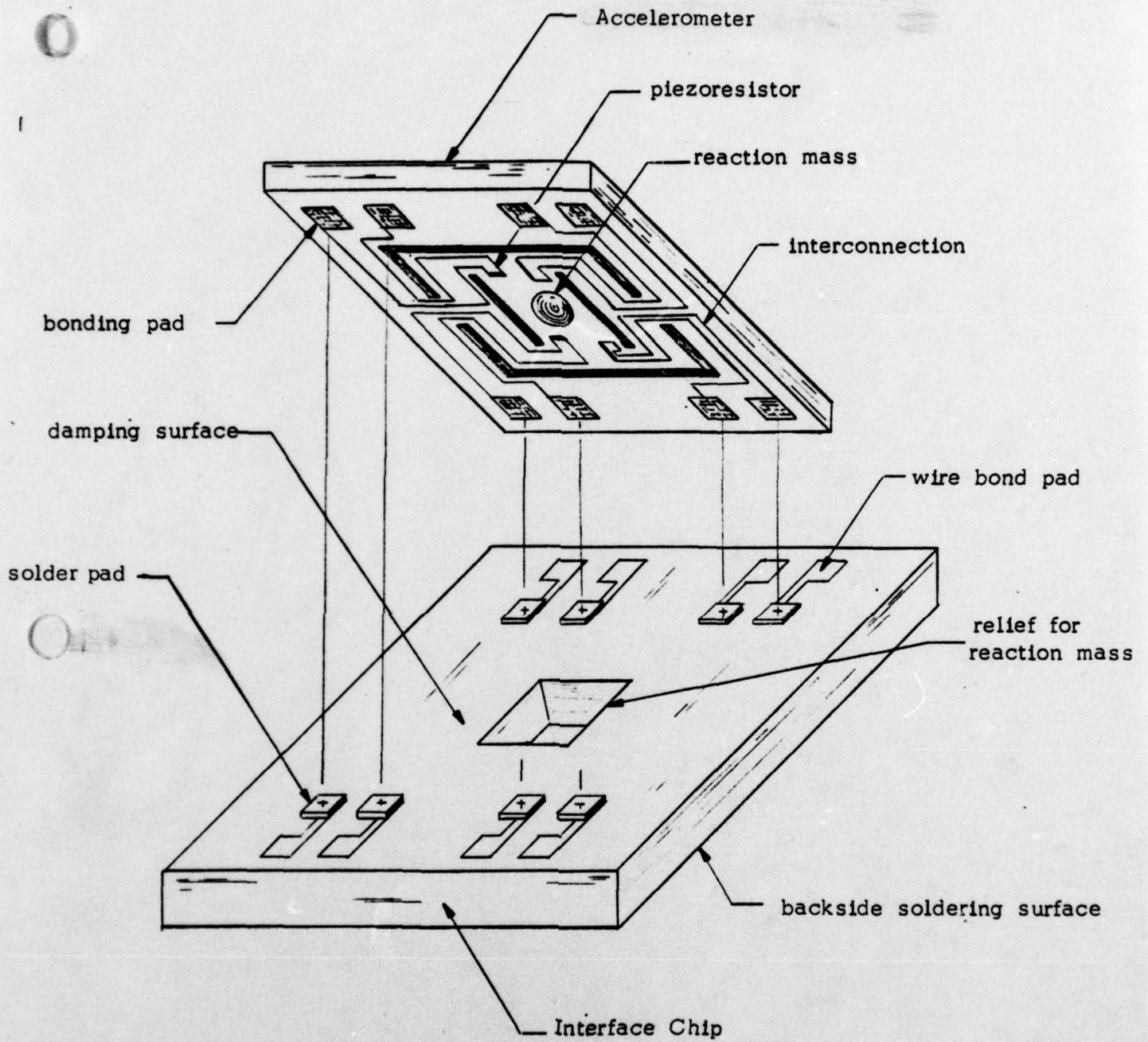
A. Interface Chip Packaging

The packaging of the transducer must satisfy the following conditions.

1. Insensitivity to thermal transfer
2. As a navigation accelerometer the membrane must be critically damped.
3. The transducer chip must be protected from corrosive or electrically conductive environments.

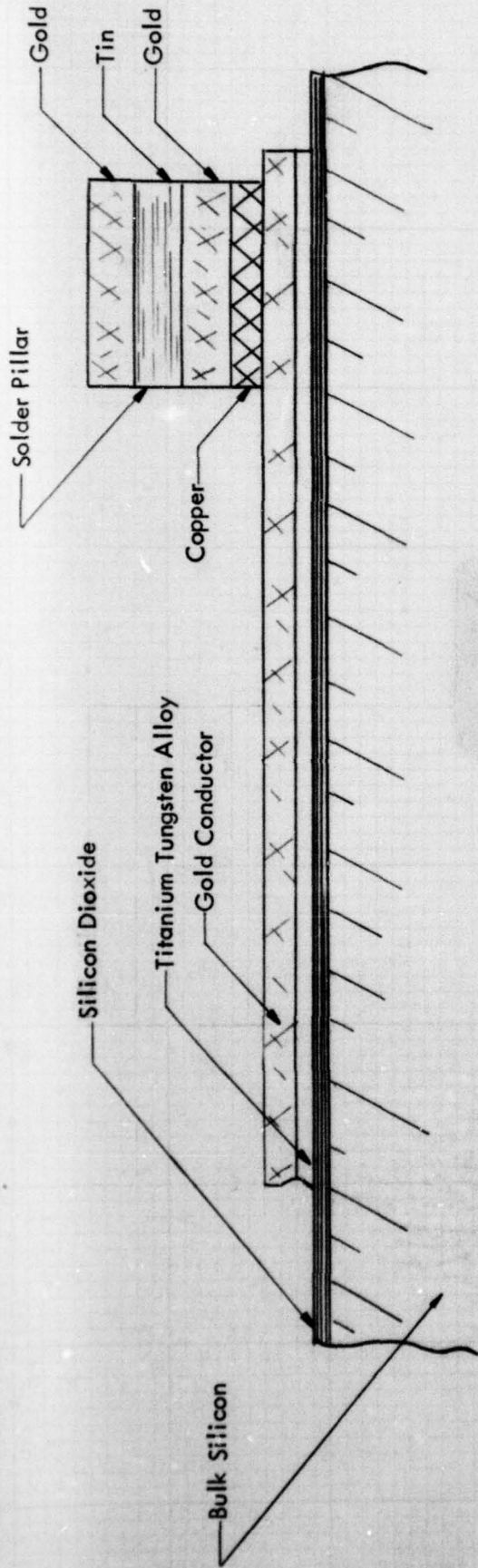
The interface chips are manufactured using a metallurgy similar to that incorporated on the accelerometer chip. The inner circle of pads are electroplated with successive layers of gold and tin. When the sensor chip is aligned and placed in contact with the interface chip and heated above the gold-tin eutectic (280°C), the interface chip solders itself to the gold bumps. These are the electrical leadouts on the accelerometer chip.

The silicon interface chip allows for a rugged transition from the transducer to the package media in the following manner. The transducer is "flip chip" bonded to the interface chip. The structure of the solder bumps is made so that a 12 μ air gap remains between transducer and interface chip after bonding. This provides damping when the transducer is packaged as an inertial sensor. Also, this bonding technique assures a minimum of thermal coupling between the transducer and the package. The interface chip assembly is then tested for both mechanical and electrical integrity. The assembly is solder attached to the package cavity and then is wire bonded to the package pads. The hermetic sealing of this bonded assembly completes the packaging.



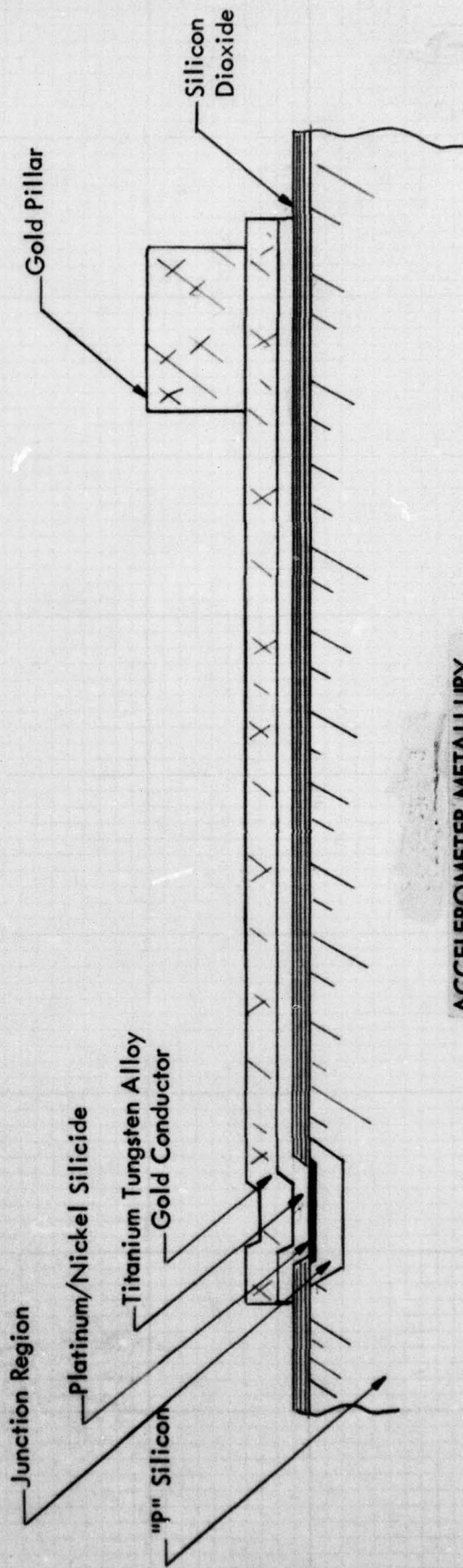
INTERFACE CHIP PACKAGING

Fig. 9



INTERFACE CHIP METALLURGY

Fig. 10

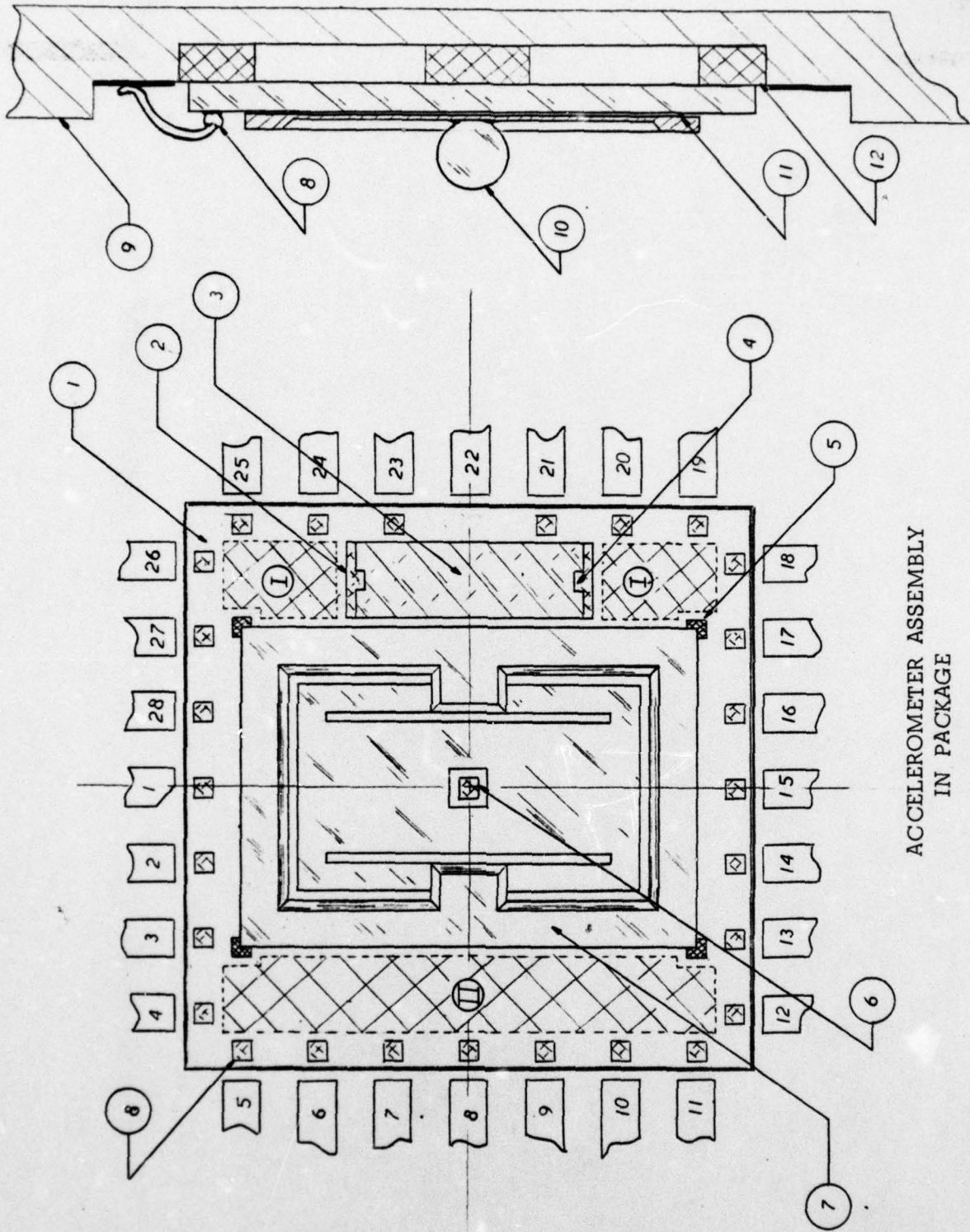


ACCELEROMETER METALLURGY

Fig. 11

MK III
TRANSUCER ASSEMBLY
IN
28 PIN D.L.P.

- 1 - Interface Chip
- 2 - Resistor Endpiece
- 3 - Bridge Trim
- 4 - Bond Pad
- 5 - Align Mark
- 6 - Center Pad
- 7 - Transducer Chip
- 8 - Bonding Pad
- 9 - Ceramic Package
- 10 - Reaction Mass
- 11 - Flip Chip Bond
- 12 - Thermal Insulator
- I - Op. Amp Regions
- II - Temp. Circuit Regions



ACCELEROMETER ASSEMBLY
IN PACKAGE

Fig. 12



Mk II/ Interface Chip Assemblies

Fig. 13

B. Damping Investigation

It was recognized early in the design program for our accelerometer that some form of damping would be required to overcome the strong natural mechanical resonance of the spring-mass system. The cantilever spring element in our accelerometer is formed from single crystal silicon and is therefore nearly an ideal spring with no losses. Coupling such an ideal spring to an unrestricted mass element yields a very high Q resonator. Practically speaking, our spring is not perfectly ideal and thus it does have some small amount of loss which limits the resonance to a finite Q. For example, a typical Mk II accelerometer housed in a conventional INB package, shows a resonant frequency of 700 Hz and a Q of 750.

The method used to determine the resonant frequency and Q of the accelerometer involves applying an impulse force to its case and observing a decaying sinusoidal signal at the output of the electronic amplifier with an oscilloscope. The resonant frequency of the accelerometer is the observed frequency of the sinusoid. The Q is calculated by counting the number of cycles it takes for the waveform to decay to e^{-1} (37%) and then using the relationship

$$Q = \pi N$$

where N = no. of complete cycles to decay to e^{-1}

$$\pi = 3.1416$$

The initial method we chose to damp our transducer was a "squeeze film" technique. This method is based on the principle that two flat plates in close proximity (interface chip assembly) moving together with some velocity, will exert a force on each other due to the separating medium (a gas) "squeezing" out from between the plates. The exerted force, between the interface chip and sensor membrane in our case, is proportional to the closing velocity of the two surfaces and is thus an ideal mechanical damping mechanism.

The following theoretical derivation of "squeeze film" damping was contributed by Prof. Dan DeBra of Stanford University. The damping model is based on rather restrictive assumptions and is thus primarily useful for first order calculations.

$$F_{\text{damping}} = b h$$

where F_{damping} = force between plates
b = damping constant
h = closing velocity of plates

b is determined from

$$b = 4/3 \mu W L^3/H^3$$

where μ = viscosity of gas
W = length of membrane
L = 1/2 width of membrane
H = separation

The damping performance of the system is characterized by its Q or alternatively by δ , the damping coefficient.

$$\delta = b/m2w_n$$

where m = total free mass
 w_n = natural resonant frequency in rad/sec

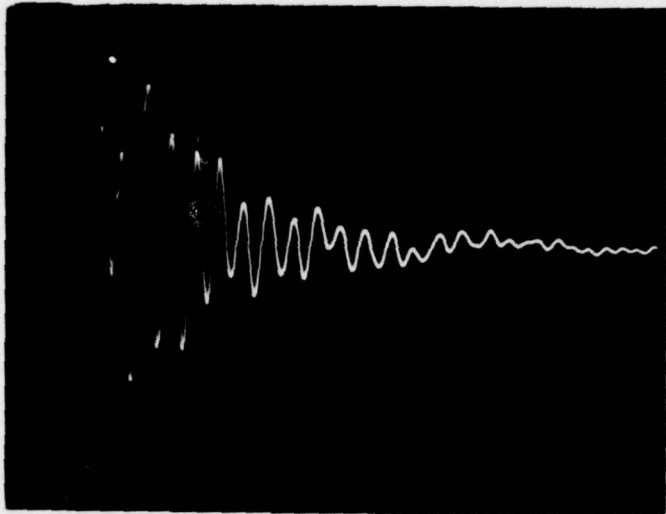
since $Q = 1/2 = m w_n/b$

Evaluating these expressions for typical values encountered in our transducer system yields

$$\delta = .48$$
$$Q = 1.04$$

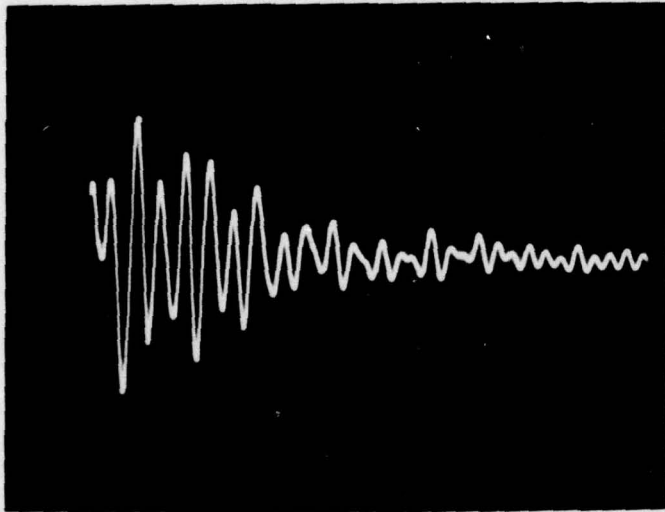
These numbers represent very acceptable performance for a damped system.

Experimentally, the performance of the "squeeze film" damping technique is not as good as expected. Tests show that in a one atmosphere nitrogen environment, the resonant frequency is 900 Hz and the Q is 16. To test the effect of the damping, the tests were repeated in an evacuated enclosure. The resonant frequency remained essentially the same, while the Q is jumped to 90. Thus there is a damping mechanism using the "squeeze film" technique, but presently the magnitude is too low for an acceptable system. We hope to decrease the separation between the damping surfaces, to lower the system Q.



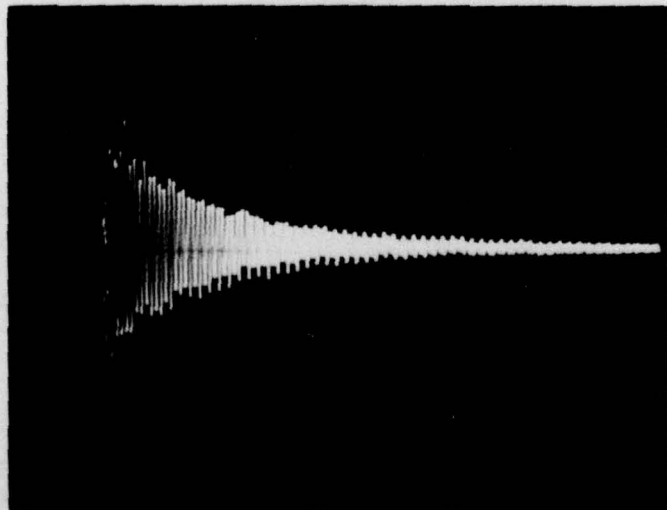
Argon - 1 atmosphere
Q = 16
Horizontal = 2 mS/Div.
Vertical = .2 volts/Div.

Fig. 14



Nitrogen - 1 atmosphere
Q = 16
Horizontal = 2 mS/Div.
Vertical = .2 volts/Div.

Fig. 15



Evacuated Chamber
Q = 90
Horizontal = 2 mS/Div.
Vertical = .2 volts/Div.

Fig. 16

SECTION V

MK II ACCELEROMETER

The layout of the heaters and sensors, with respect to the piezoresistors, in the Mk II accelerometer was based on the following considerations:

1. It must be assumed that the heat sources introduce no thermal gradients that cause unbalance of the bridge.
2. The most desirable situation is that the bridge and the temp. sensor reside at the same temperature or at worst case, a temperature which differs by a constant. Thus if we insure that the temp. sensors' temperature is constant, the bridge temperature is constant.
3. The sensor and heater must be located as closely to one another as possible. This will permit the use of large loop gain, and will in turn result in precise sensor stabilization.

The heater transistors are located as shown on Figure 19 with the temp. sensors adjacent. The following points are stressed.

1. The heat flux along the membrane arms is the power dissipated in the bridge or approximately 5 mW. The net thermal resistance of this path is about 300°C/W. This 25 μ thick silicon membrane has a thermal sheet resistivity of 200°C/W.

Thus the ΔT will be only 1.5°C between the heater region and the piezoresistor areas. The important fact is that this difference is constant and will not vary with ΔT ambient.

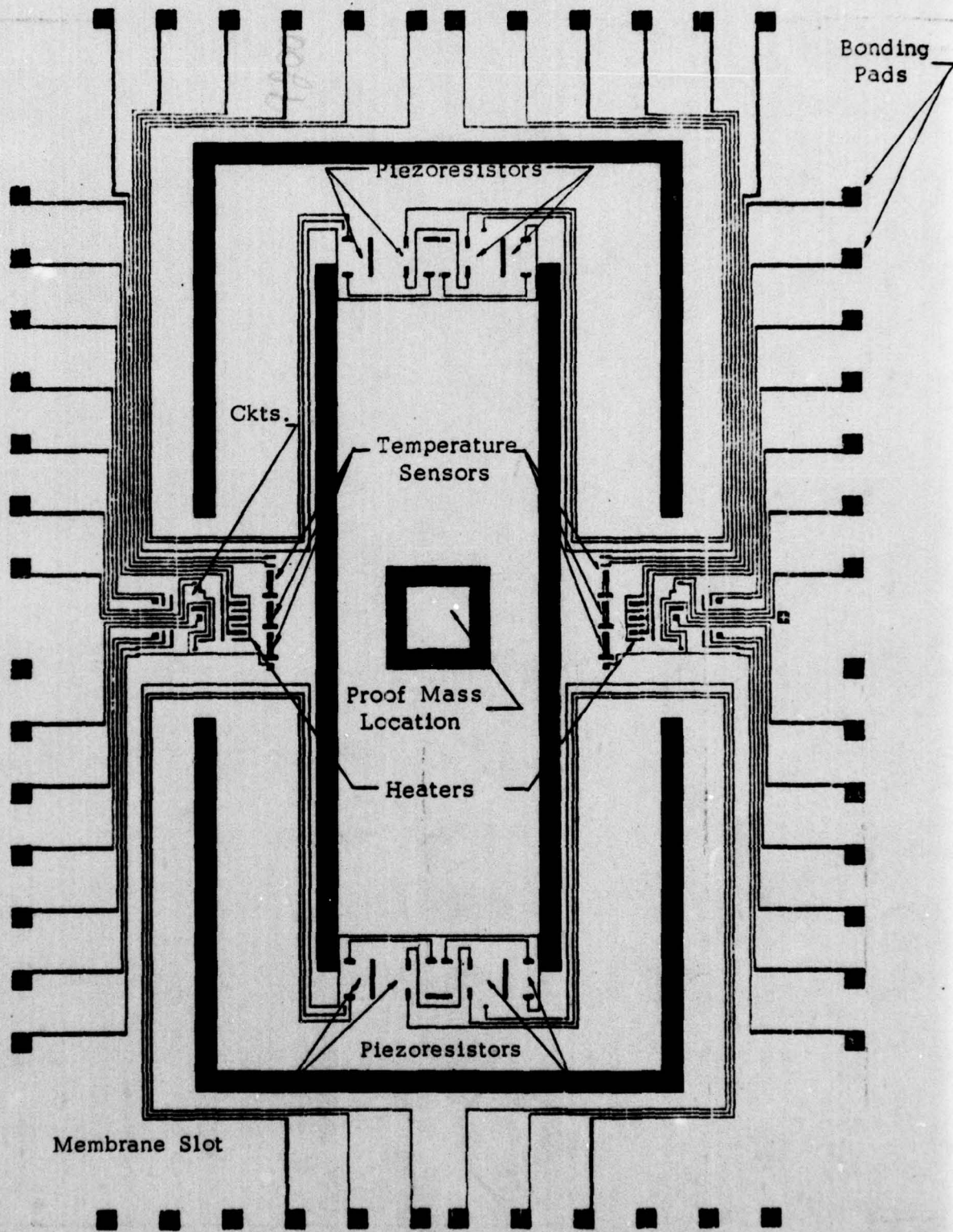
2. The sensor and heater are adjacent which allows high loop gain.
3. A critical factor is that the two heaters must dissipate equal power. If this does not happen, there will be a ΔP which is proportional to T_A , and a ΔT will be produced across the membrane. Further, if the accelerometer packaging is relatively non-uniform in thermal symmetry, a similar event will occur.

Therefore it is best to stabilize the opposing sides independently. The difference in T_{chip} between them will be set by V_{BE} mismatch δ , and holding within 2 mV, the ΔT will be less than 1°C.

The piezoresistors in the Mk II were changed to a "zero TC" ion implanted type, and increased in width to 40 μ to improve statistical matching. Each resistor was placed in an isolated tub, since an epi process was now being used for the heat control elements, with an individual tap for each isolated region. The piezoresistors were placed orthogonal to each other (as in the Mk I), but a common centroid geometry was used to minimize temperature gradients. Each resistor consisted of 4 subsections connected in series to form the whole 12 square piezoresistor.

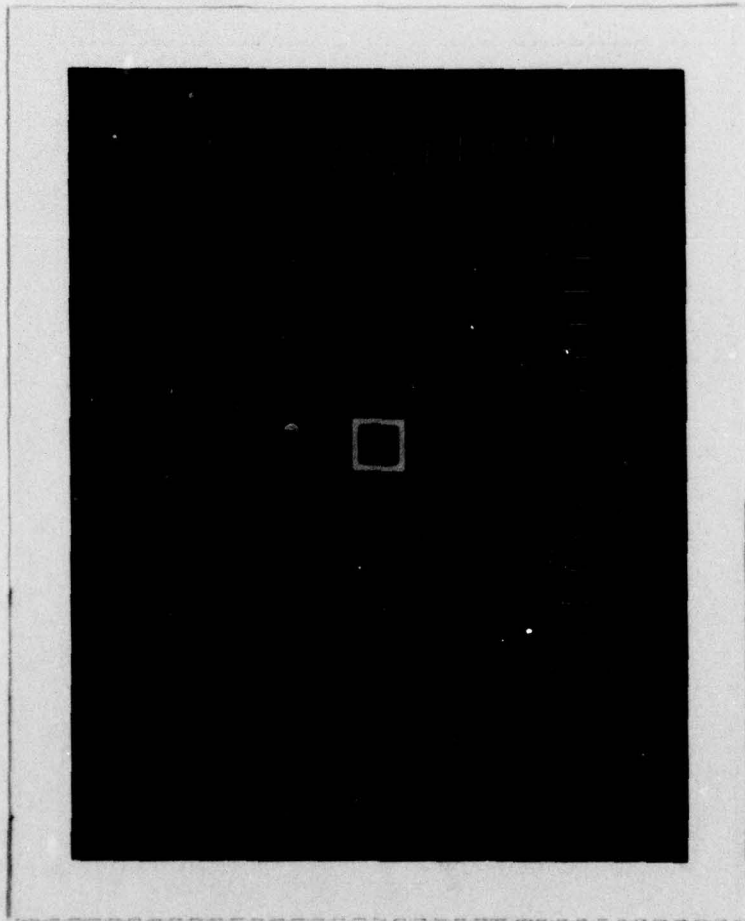
MEMORANDUM (continued)

The dual heat control elements consisted of a large npn transistor for heating, four diodes for heat sensing, and a zener reference for accurate control. The heat control elements were not placed on the membrane, but in the thick region on either side of the membrane.



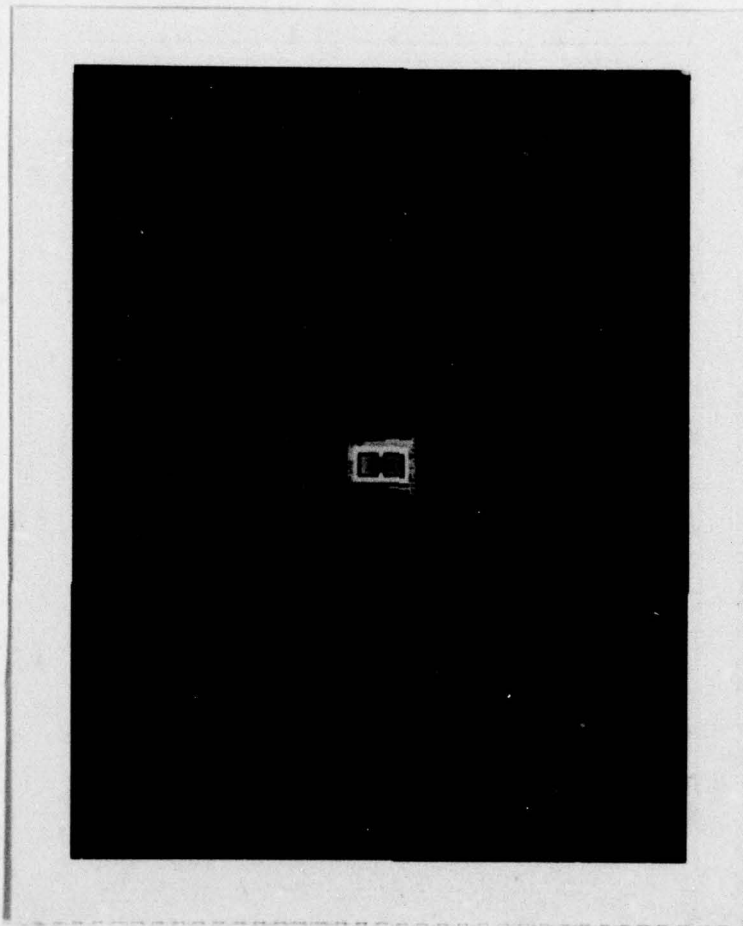
Mk II Accelerometer Layout

Fig. 19



Mk II Accelerometer
Double Ended Orthogonal Piezoresistors

Fig. 17



Hermetic Enclosure Interface Chip
Package Assembly

Fig. 18

MK II ACCELEROMETER
DYNAMIC TEST RESULTS FROM STANFORD UNIVERSITY

The first dynamic test results of the folded cantilever accelerometer were generated by Stanford University 11/15/76. At our request, they performed two dynamic tests:

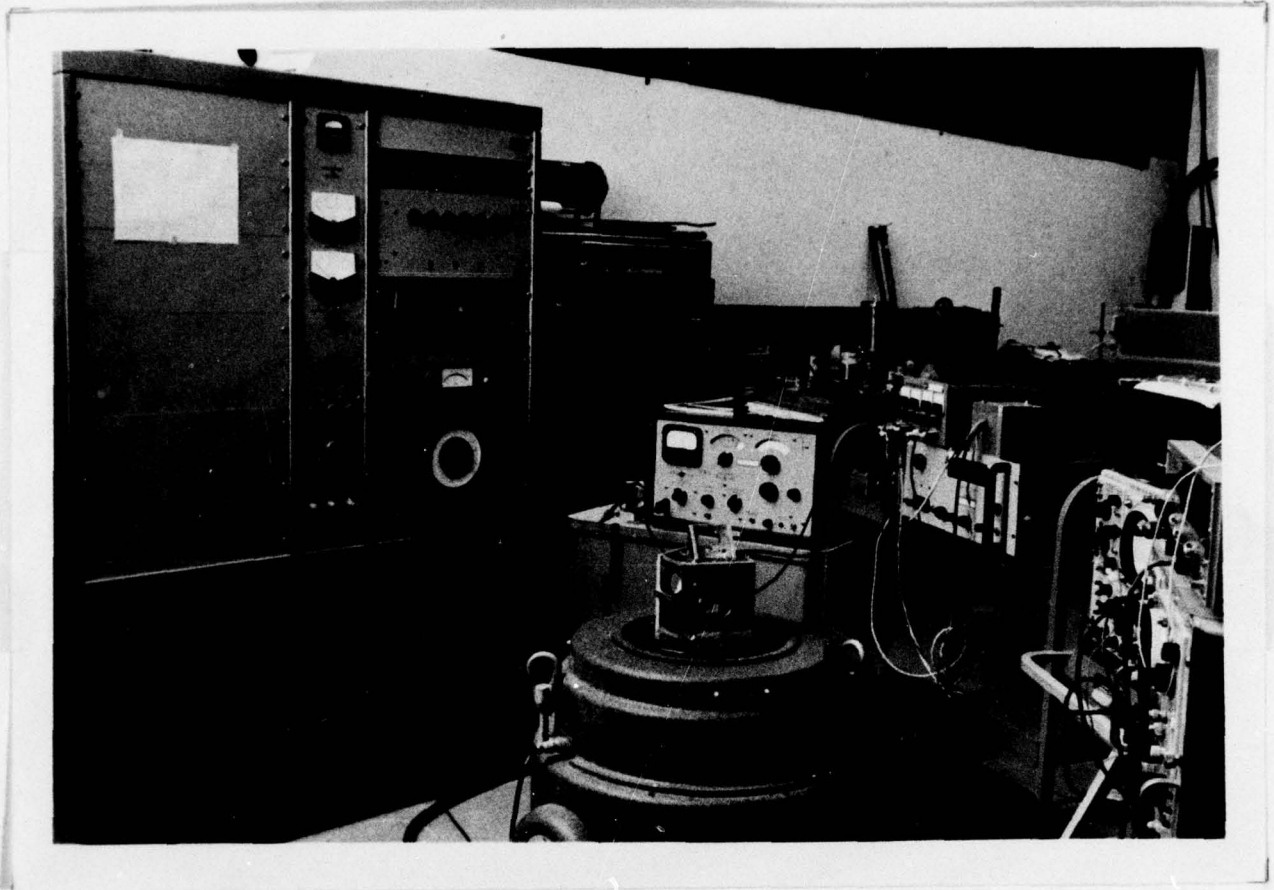
1. Linearity Response at 100 Hz
2. Frequency Response at 1 g

The results of these tests should be considered "preliminary" in nature, since the vibration table was not optimized for the large dynamic range required, and the reference Bell accelerometer was not available for an accurate measurement standard. In spite of these deficiencies, the results are very promising, and show good progress toward contract goals.

Fig. 21 and Fig. 22 show the output of the accelerometer, as measured on the wave analyzer, as a function of applied acceleration at 100 Hz. The wave analyzer was set at 100 Hz to read only the fundamental vibration frequency. The acceleration standard for these measurements was an internal velocity pickup in the vibration table. The abrupt discontinuity at 10 g was due to a range change on the vibration table control panel. The graph is quite linear up to 15 g despite the probable inaccuracies in the measurement system.

Fig. 23 and Fig. 24 show the output of the accelerometer as a function of an applied acceleration of 1 g at frequencies between 30 Hz and 2000 Hz. The vertical axis is shown in dB to accommodate the large response at the resonant frequency. The output values were obtained by tuning the wave analyzer to the fundamental shake frequency at each measurement point.

Fig. 24 shows several interesting features. First, it has the classic shape of an underdamped second-order system. It appears to have a resonant frequency of 1320 Hz and a Q of roughly 56. Alternate impulse tests have shown the unit to have a natural resonant frequency of 1000 Hz and a Q of 16. There is a discrepancy here which will have to be resolved. Second, the frequency response is quite flat with the exception of a 2-3 dB perturbation at around 100 Hz. This correlates well with impulse tests which show a secondary natural mode at 100 Hz



View of the electronic equipment showing the control panel (left) for the vibration table.

Fig. 20 - 3

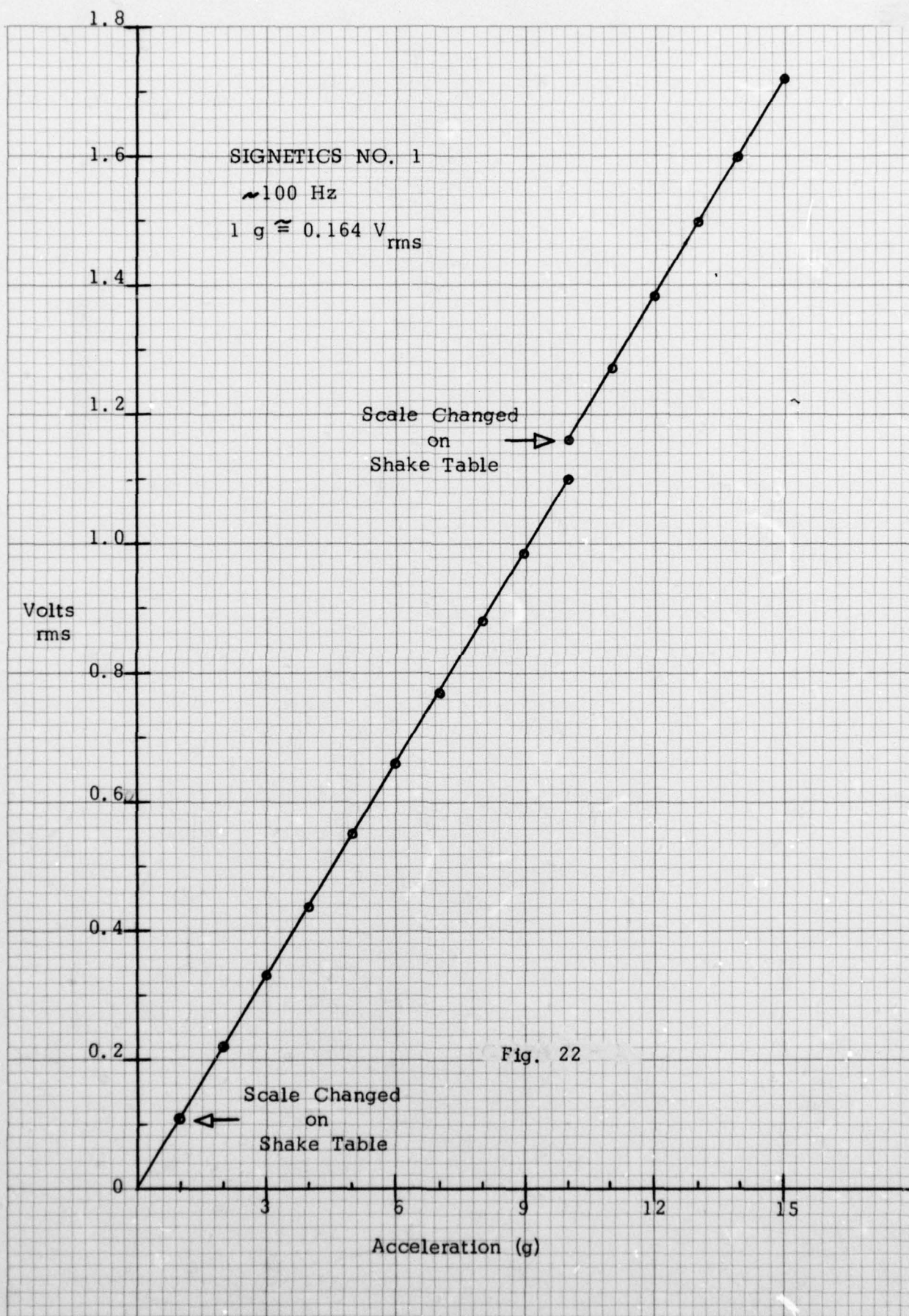
SIGNETICS No. 1 - 100 Hz Response

<u>Acceleration</u>	<u>Reading (volts)_{rms}</u>	(from harmonic analyzer)
0.1 g	0.012	
0.3	0.0335	
0.5	0.056	
0.7	0.079	
0.9	0.100	
[1.0	0.110]	(scale changed on shake table)
1.0	0.115]	
1.2	0.137	
1.6	0.180	
2.0	0.224	
2.6	0.287	
3.0	0.333	
3.6	0.398	
4.0	0.440	
4.5	0.492	
5.0	0.552	
5.5	0.610	
6.0	0.670	
6.5	0.720	
7.0	0.773	
7.5	0.825	
8.0	0.880	
8.5	0.930	
9.0	0.980	
9.5	1.04	(scale changed on shake table)
[10.0	1.09]	
10.0	1.12]	
11.0	1.27	
12.0	1.38	
13.0	1.49	
14.0	1.60	
15.0	1.73	

Fig. 21

46 0700

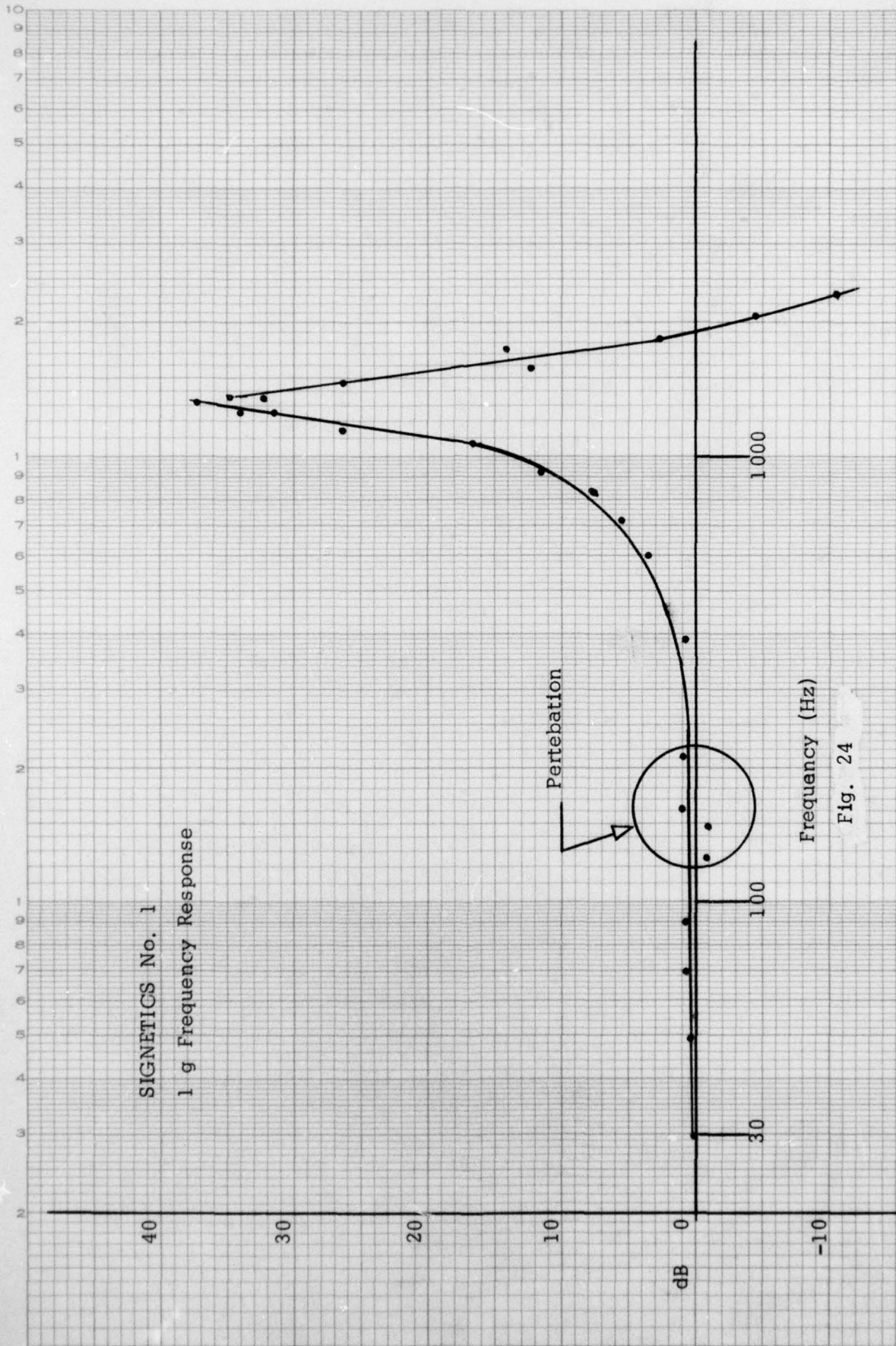
K·E 10 X 10 TO THE INCH • 7 X 10 INCHES
KEUFFEL & ESSER CO. MADE IN U.S.A.



SIGNETICS No. 1 - Frequency Response at 1 g

<u>Frequency</u>	<u>Reading (volts)_{rms}</u>	(from harmonic analyzer)
30 Hz	0.170	
50	0.167	
90	0.174	
125	0.145	
145	0.145	
160	0.182	
210	0.175	
260	0.178	
380	0.190	
470	0.213	
590	0.253	
700	0.310	
800	0.400	
900	0.600	
1050	1.10	
1130	3.25	
1250	5.80	
1280	6.10	
1320	8.00	
1350	3.20	
1450	0.66	
1550	0.79	
1700	0.222	
1800	0.157	
1900	0.100	
2000	0.070	
2200	0.048	

Fig. 23



MK II ACCELEROMETER
CRITIQUE AND RECOMMENDATIONS

Although the Mk II performed as expected in dynamic stress where the ambient temperature conditions did not vary more than a few degrees, the temperature control features were disappointing because of the following basic design flaws.

1. Poor thermal coupling between heat sensors and piezoresistors.
2. Breakdown and surface inversion in piezoresistor area of the chip.
3. Floating substrate (not able to be grounded).
4. Low thermal resistance with interface chip packaging due to large number of pads (52 as opposed to the 26 required).
5. Poor piezoresistor design for matching and minimum differential TCR.
6. Large sensitivity to oxide prestress.

The reason for the poor coupling has been isolated as thermal conduction through the air medium and high thermal sheet resistance of the silicon membrane. Using a simple transmission line analogy, it has been possible to calculate the temperature on the membrane as a function of position. The calculations agree closely with measured data, and indicate a temperature loss of 25°C from the sensor to the resistor area.

Due to the large temperature gradients on the membrane, it was necessary to redesign the transducer to place four independent heater/sensor pairs on the membrane, next to each piezoresistor. Many of the lines are common, so that actually there will be a reduction in the complexity of the leads to the membrane. However, even though the new design will only use one end of the membrane for circuits, much more metal will be added to the whole membrane than previously. We hope that this will have a negligible effect on the linearity of the spring, and provide a small amount of damping.

The acceleration and temperature sensitivity of the Mk II was comparable to the Mk I. The ion implanted resistors retained the same nonlinearities and stress sensitivity as the diffused units, but they did not improve the temperature matching, as we had hoped. A further analysis into the problem showed that we had overlooked a "built-in" stress phenomenon in the membrane, which was due to the unequal coefficients of expansion of silicon and silicon dioxide. The membranes were highly curled in response to this stress, which became increasingly obvious as we attempted to make units with thinner membranes. Further analysis showed that it would not be possible to reduce the prestress to zero,

MK II ACCELEROMETER
CRITIQUE AND RECOMMENDATIONS (continued)

thus the only alternative was to reduce the sensitivity of the resistors to this mechanism. Our design approach to this problem is discussed in the next section under the Mk III Prototype.

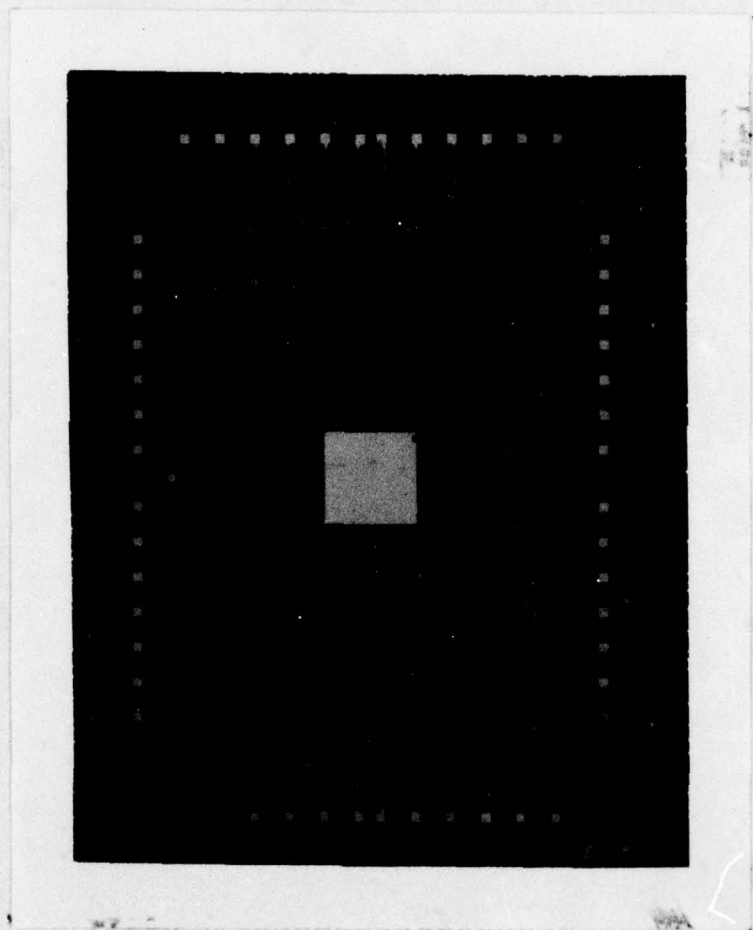
A membrane temperature analysis is presented in depth to explain the inadequate thermal control performance of the Mk II accelerometer.

SECTION VI
MK III PROTOTYPE
DOUBLE ENDED UNIDIRECTIONAL PIEZORESISTORS

It was suspected that the consistently large differential TCR of the bridge piezoresistors was due to a silicon/silicon dioxide (Si/SiO₂) prestress mechanism in the Mk I and Mk II accelerometers. The prestress is created in the fabrication of these devices since SiO₂ is thermally grown at elevated temperatures and has a lower coefficient of thermal expansion than silicon. Thus as it cools, the silicon shrinks faster than the oxide, creating a stress in the interface region. The magnitude of the stress is greater than 10⁷ dyn/cm² and causes visible bending of the membrane (bi-metal effect).

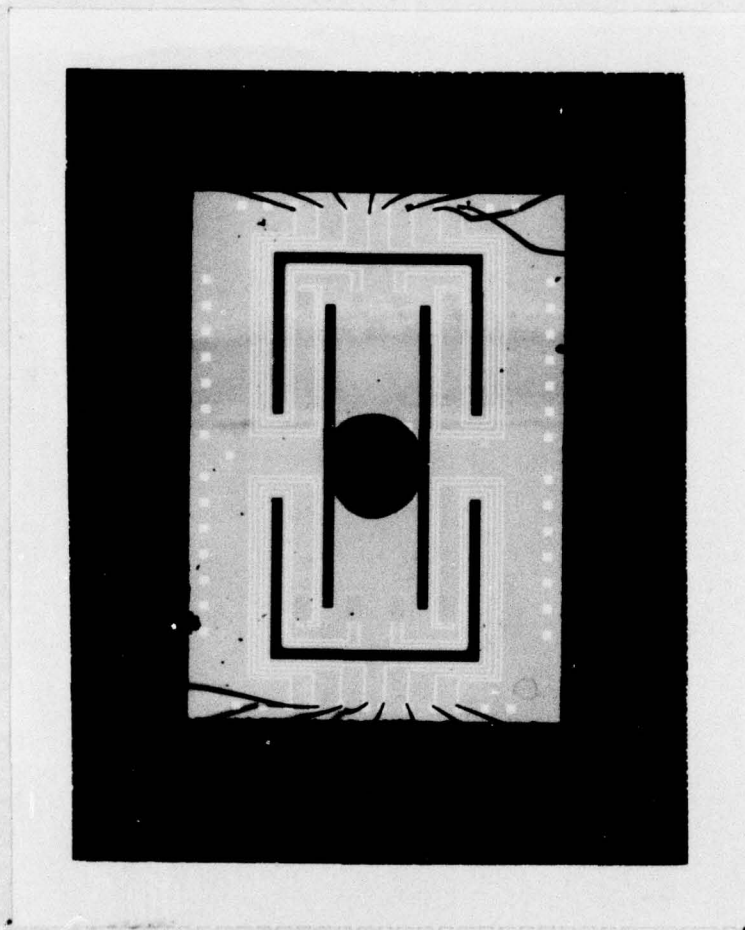
When piezoresistors are inserted into this prestress at right angles to each other, the stress causes one resistor to increase and the other to decrease, i. e. poor resistor matching. The piezoresistor bridge responds to prestress as it would to an acceleration induced stress. It "thinks" it is seeing an acceleration of 10-20 g's with no externally applied signals. The bias stress or prestress due to Si/SiO₂ interaction is fairly independent of temperature in the military range. However, the piezo-coefficient (π), which relates change in resistance to stress is strongly temperature dependent and varies roughly as 1/T (K°). Thus the piezoresistors see a change in resistance which is a function of temperature and their orientation. This creates a differential TCR over and above the basic statistical differential TCR of the bridge.

To try to overcome the problems created by prestress (poor resistor matching and large differential TCR) the Mk III prototype accelerometer was designed. In the new design, piezoresistors were all placed in the same direction to cancel the effect of the prestress. The resistors that were originally at right angles to the long dimension of the membrane, were moved from areas of tension to areas of compression, to preserve the acceleration induced signal. See Fig. 28.



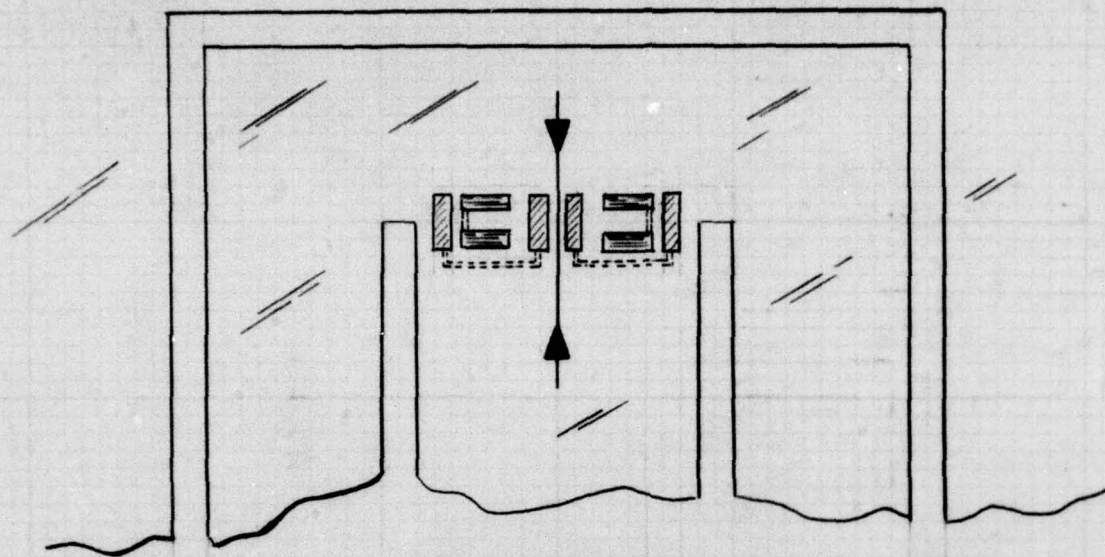
Mk III Prototype Accelerometer

Fig. 25



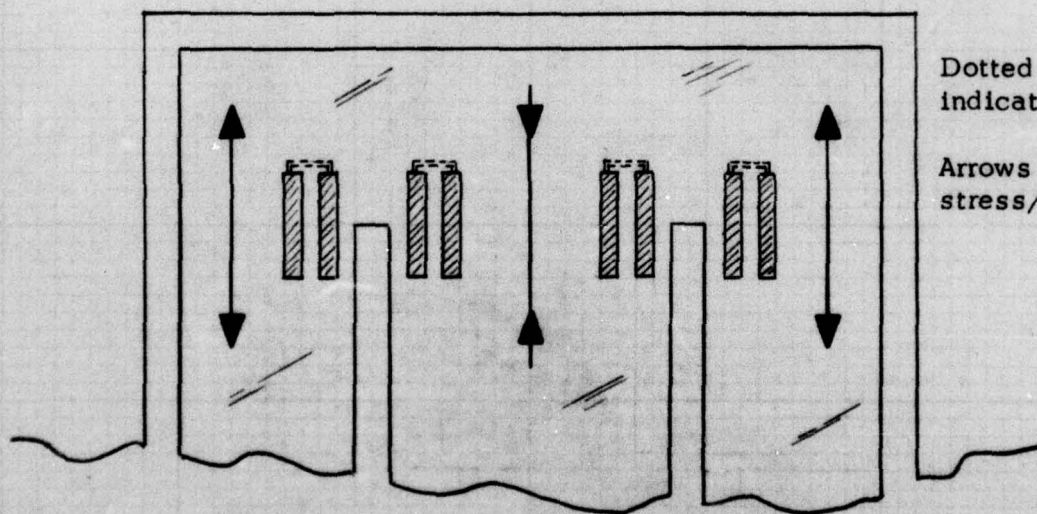
Packaged Mk III Prototype Accelerometer

Fig. 26



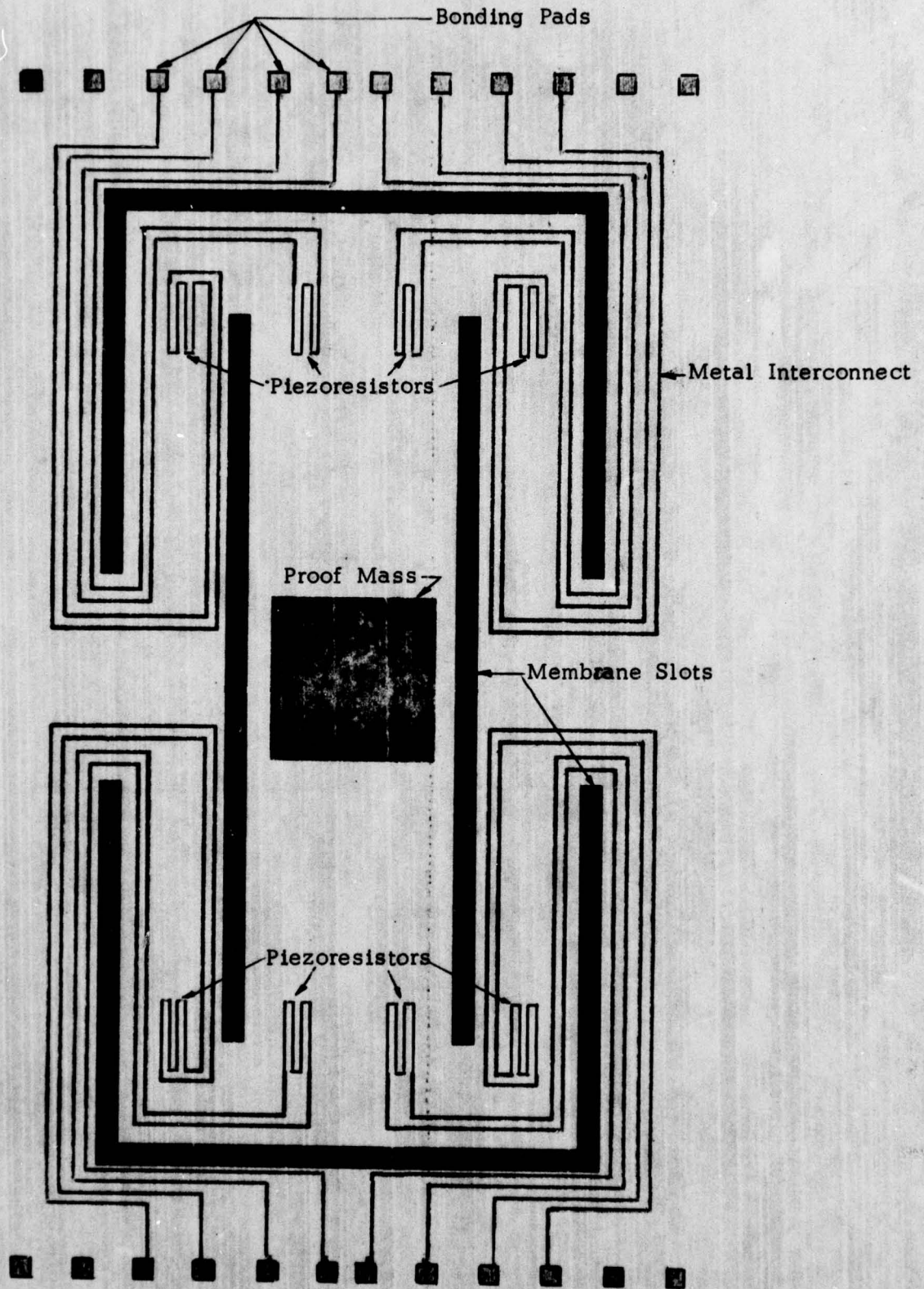
Mk II Resistor-Membrane Geometry

Fig. 27



Mk III Resistor-Membrane Geometry

Fig. 28



Mk III Prototype Accelerometer Layout

Fig. 29

TEST RESULTS/RECOMMENDATIONS

The Mk III Prototype was able to consistently reduce the differential temperature coefficient of the bridge by a factor of three to four over typical Mk I and Mk II performance. It was not completely successful, however, since an additional factor of five to ten improvement is necessary for a truly wide dynamic range device. The fact that we were able to reduce it at all is significant, because it indicates that our theoretical analysis was basically correct. Any additional improvements in the temperature sensitivity will have to incorporate a three dimensional stress analysis of the membrane and a vastly superior photolithographic technique such as electron beam.

The stress sensitivity, nonlinearities, and the excess noise of the Mk III Prototype was basically the same as both the Mk II and Mk I devices. However, the resistor placement scheme did have a drastic effect on the misalignment angle of the accelerometer. Previously, this angle was negligible (much less than a degree) and was thought to be due to misalignments in the packaging and test equipment. Now, in the Mk III, this angle is 10-20 degrees and introduces a serious question as to the origin of the phase error. Additional experiments with static and dynamic excitation will have to be used to evaluate the effect of the misalignment. Figure 30 shows the phase shift in the relative output signal that is typical of the Mk III design which incorporates unidirectional resistors (compare with Mk I and Mk II).

TRANSDUCER NON-LINEARITY VS ROTATION

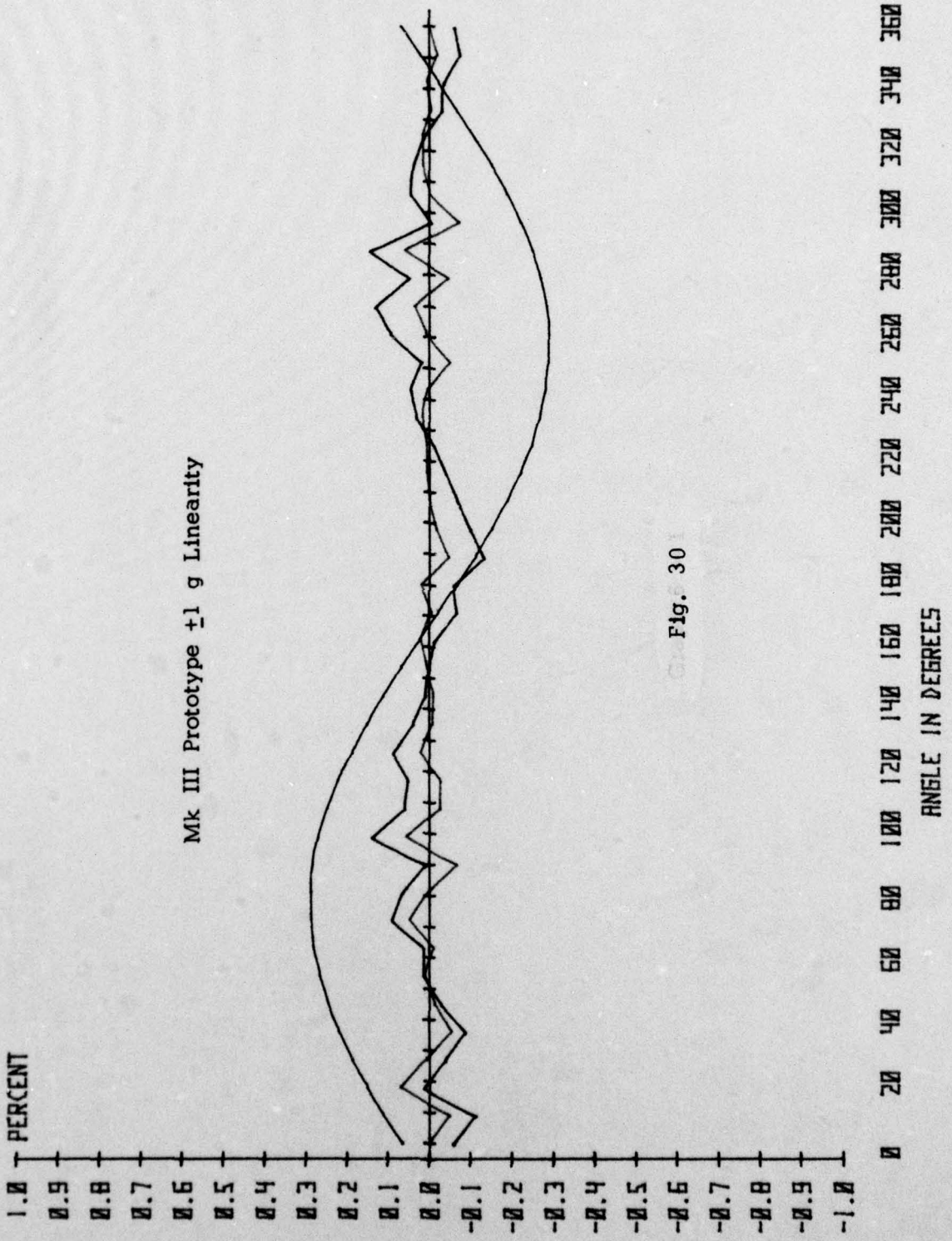


Fig. 30

SECTION VII

THE MK III ACCELEROMETER SINGLE ENDED RESISTOR BRIDGE WITH TEMPERATURE CONTROLLED CIRCUITRY

The deficiencies of the Mk II accelerometer design have resulted in a piezoresistive sensor with the following problems:

- 1) a large sensitivity to temperature,
- 2) a poor temperature control system,
- 3) a large sensitivity to environmental effects like voltage, charge, moisture, etc.

The Mk III design attempts to solve the above problems as well as add some badly needed features to improve yield and facilitate testing.

To solve problem (1) in the Mk II sensor, the Mk III design uses an alternate placement of resistors on the sensor membrane. Figure 33 shows two of four piezoresistors in the Mk II sensor layout, and Figure 34 shows all four piezoresistors in the improved Mk III design. In the Mk II design, each piezoresistor was broken into four segments (3 squares per segment) which were placed at right angles to each other in a common centroid geometry. The entire pattern was located in an area of tensile stress so that the segments parallel to the membrane slots would increase in resistance, and the segments perpendicular to the slots would decrease in resistance. A duplicate geometry was located on the opposite end of the membrane to make a total of four bridge resistors. The fact that the resistor segments were oriented at right angles to each other and that there was a large bias stress in the Si/SiO₂ interface, created both a differential temperature coefficient in the bridge and excessive resistor mismatching. This was discussed in detail under "Piezoresistor Technology" in 100 D.A.C. To alleviate the problem in the Mk III design, the piezoresistors were all moved to one end of the membrane, and those resistors that were previously perpendicular to the slots were moved to areas of compressive stress to retain the same decrease in resistance. In Figure 34 if the center two piezoresistors are in tension, then the outer two will be in compression, and the full bridge signal is maintained. However, the Mk III design has the advantage of first order cancellation of the differential temperature coefficient due to bias stress, since the bias stress now has an identical effect on all piezoresistors and thus will be rejected by the bridge. The differential TCR of the Mk III design should be dictated entirely by statistical resistor matching, which can be controlled by advanced processing techniques.

To solve problem (2) the Mk III design uses four independent heater/sensor control loops, each in close proximity to a piezoresistor, for temperature control. The heater/sensors were moved up onto the membrane to overcome the problem encountered in the Mk II design of large heat losses due to thermal conduction to ambient. The high

thermal sheet resistance on the membrane and the thermal conduction to the air medium resulted in a large temperature drop (25°C) from the sensor to the piezoresistor area. Thus, it was impossible to regulate the temperature of the piezoresistors with any accuracy. A quad regulator was incorporated into the Mk III design to prevent temperature gradients from unbalancing the piezoresistive bridge. Each piezoresistor is closely coupled to a heater/sensor and will be accurately temperature controlled.

The third problem with the Mk II design has been overcome by closer attention to process design rules, the incorporation of process monitors and the reduction in size of the sensor to fit a standard hermetic IC package. As discussed previously, the Mk II sensor had several design errors which made it difficult to use because of its large sensitivity to environmental factors. It was also difficult to test in a hermetic environment since a custom package had to be designed to house the sensor/interface chip assembly. The smaller size of the Mk III for ease of packaging, and the increased attention to the problem details in the Mk II makes Mk III a vastly improved design.

This design incorporates many novel design features which were not on the Mk II accelerometer. These additions were made to facilitate device fabrication and optimize performance. Figure 35 shows the nine areas of improvement over the Mk II design.

A. Test Structures (2)(3)(5)

Because the individual components of the accelerometer circuits are electrically interactive and physically small, it is impractical to evaluate their individual electrical parameters. In order to provide this "discreet" test capability, certain critical circuit components were scaled up to a size where they can conveniently be electrically contacted and evaluated. These test structures are as follows:

- 2 - diffused resistor
- 3 - ion implanted piezoresistor
- 5 - transistor

This technique provides us with a relatively simple means of trouble shooting the electronic characteristics of the accelerometer.

B. Depth Gauges (1)

During the front side silicon membrane slot etch process, 6 rectilinear patterns are also defined. The dimensions of these patterns are mathematically derived from the anisotropic etch predictions of <100> orientation silicon and will yield precisely controlled apexed bottoms. These patterns will etch to depths of 15 to 40 μm in 5 μm increments. The final silicon etch done from the back side of the membrane determines

the eventual membrane thickness. The sensitivity of the sensor is a direct function of the membrane thickness. Therefore it is imperative that this silicon etching be under precise control. The function of the depth gauges is to provide a visual depth reference for the control of membrane thickness. As the membrane is gradually thinned, the depth gauges will visually appear in order of their depth. Using this technique the etching operator can precisely control the final membrane thickness and accelerometer sensitivity.

C. Corner Compensation (4)

The corner compensation square placed on all outside anisotropically etched corners allows for final etched membrane having improved lateral configurations.

D. Substrate Contact (6)

The Mk II design did not have a substrate contact and because of this, testing was in some cases difficult due to charge buildup and other factors. This feature will alleviate this problem

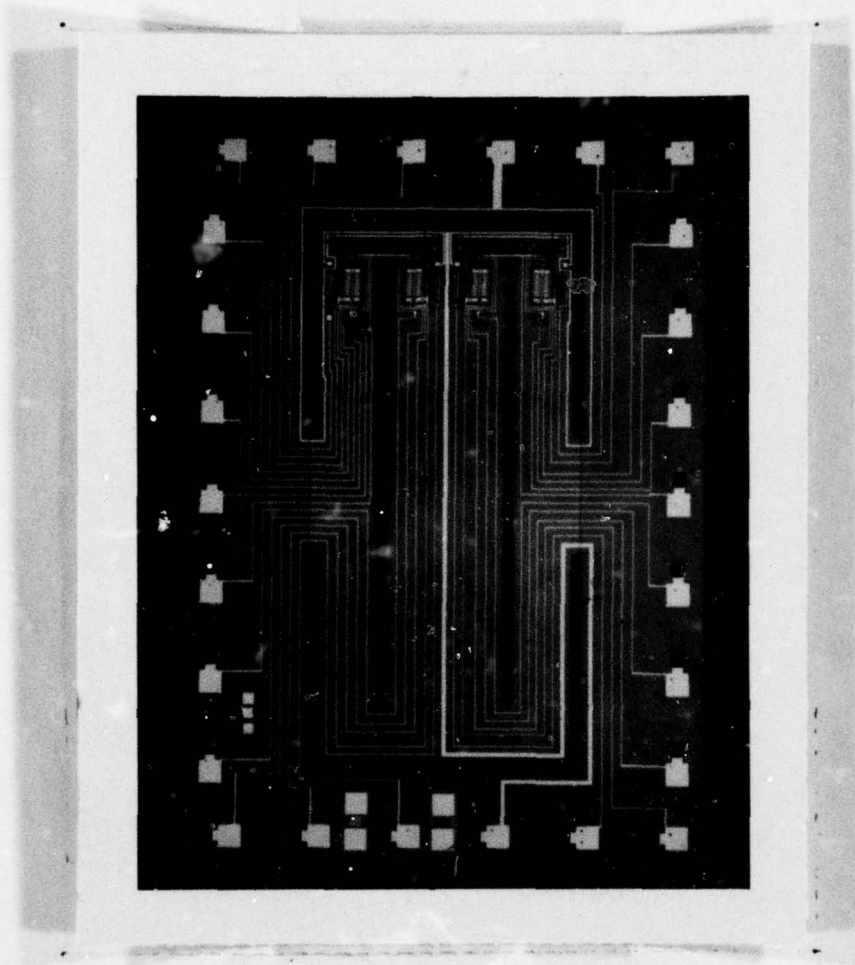
E. Dual Bond/Probing Pad (7)

The Mk II devices had to be contacted directly onto the bonding pillar during electrical testing. This deformed the soft gold pillar to such an extent that in many cases interface chip soldering could not be effected due to non-planarity. The Mk III design affords electrically continuous pads for both probe contacting and solder bonding. This will greatly enhance assembly yield.

F. Piezoresistor/Heater Location (8)(9)

The close correspondence of the piezoresistor and heater assures optimized thermal control of the accelerometer.

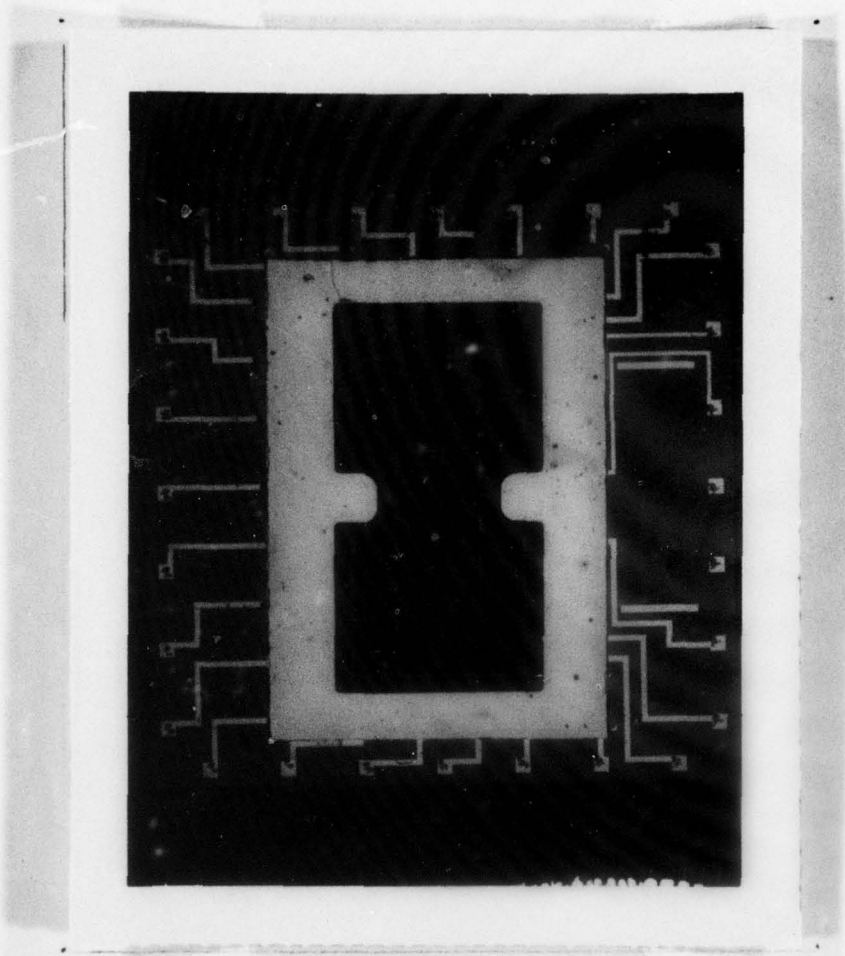
Figs. 38 through 43 show in detail the Mk III design improvements.



Mk III Accelerometer/Interface Chip Assembly

Fig. 31

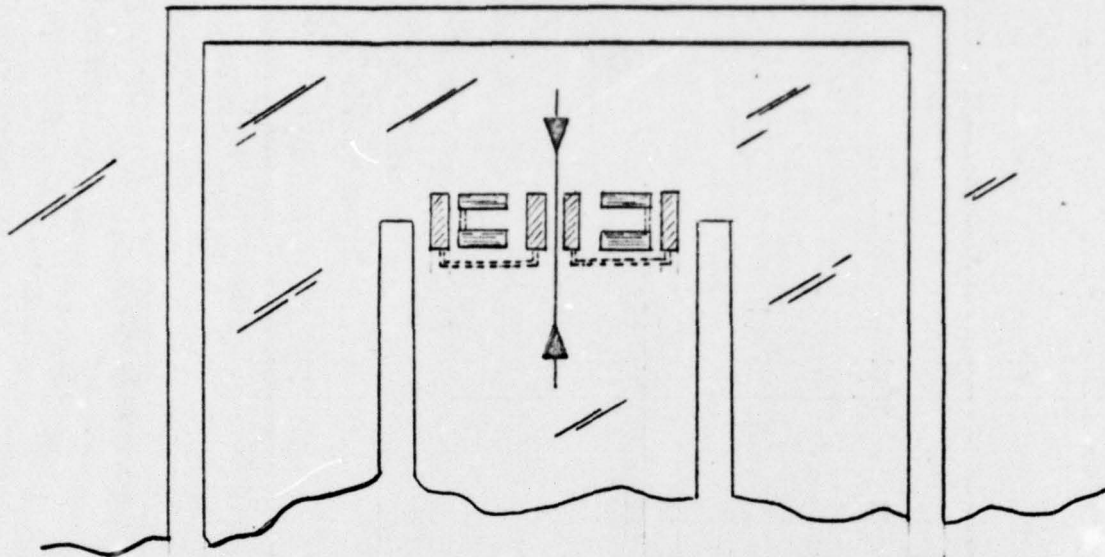
This is an overall view of the Mk III device which graphically shows the various features which make this design considerably different and simplified when contrasted with the Mk II.



Mk III Accelerometer/Interface Chip Assembly

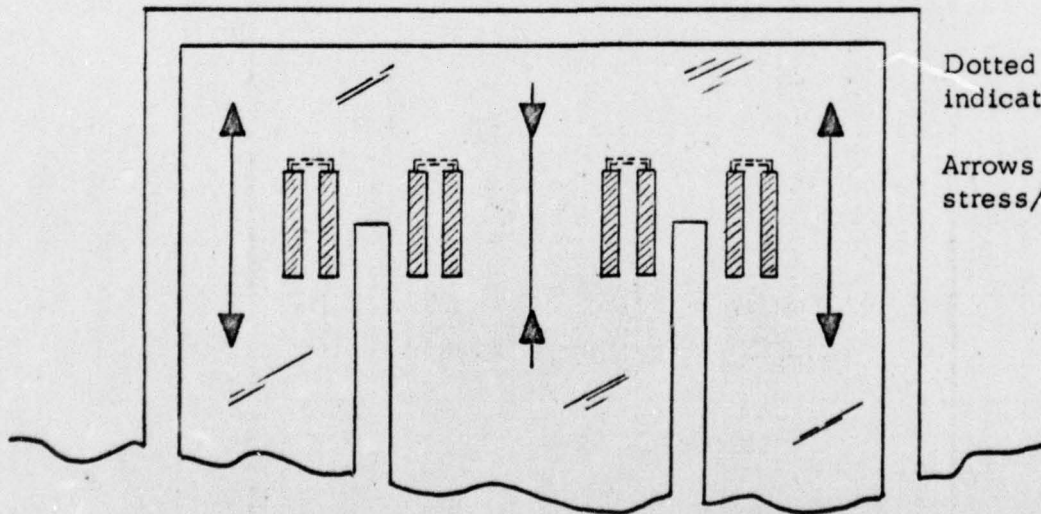
Fig. 32

This is a fully tested pre-assembly (note probe marks on the bonding pads). This pre-assembly is now ready for final assembly into a 28 pin D.I.P. The features on the membrane are the diffused collectors at the top and the membrane thickness gauges at the bottom.



Mk II Resistor-Membrane Geometry

Fig. 33



Dotted lines
indicate metal links

Arrows show dynamic
stress/strain directions

Mk III Resistor-Membrane Geometry

Fig. 34

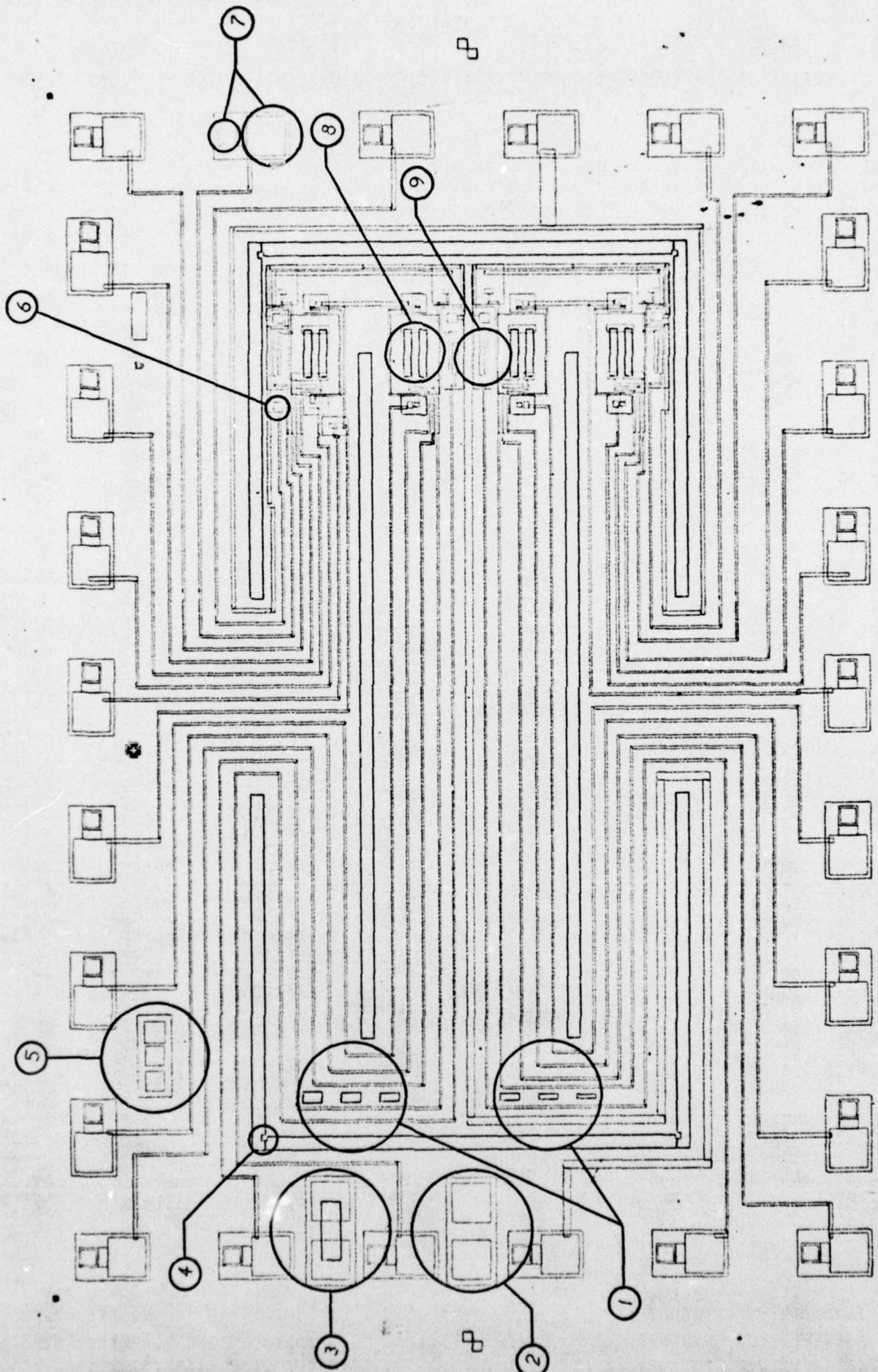
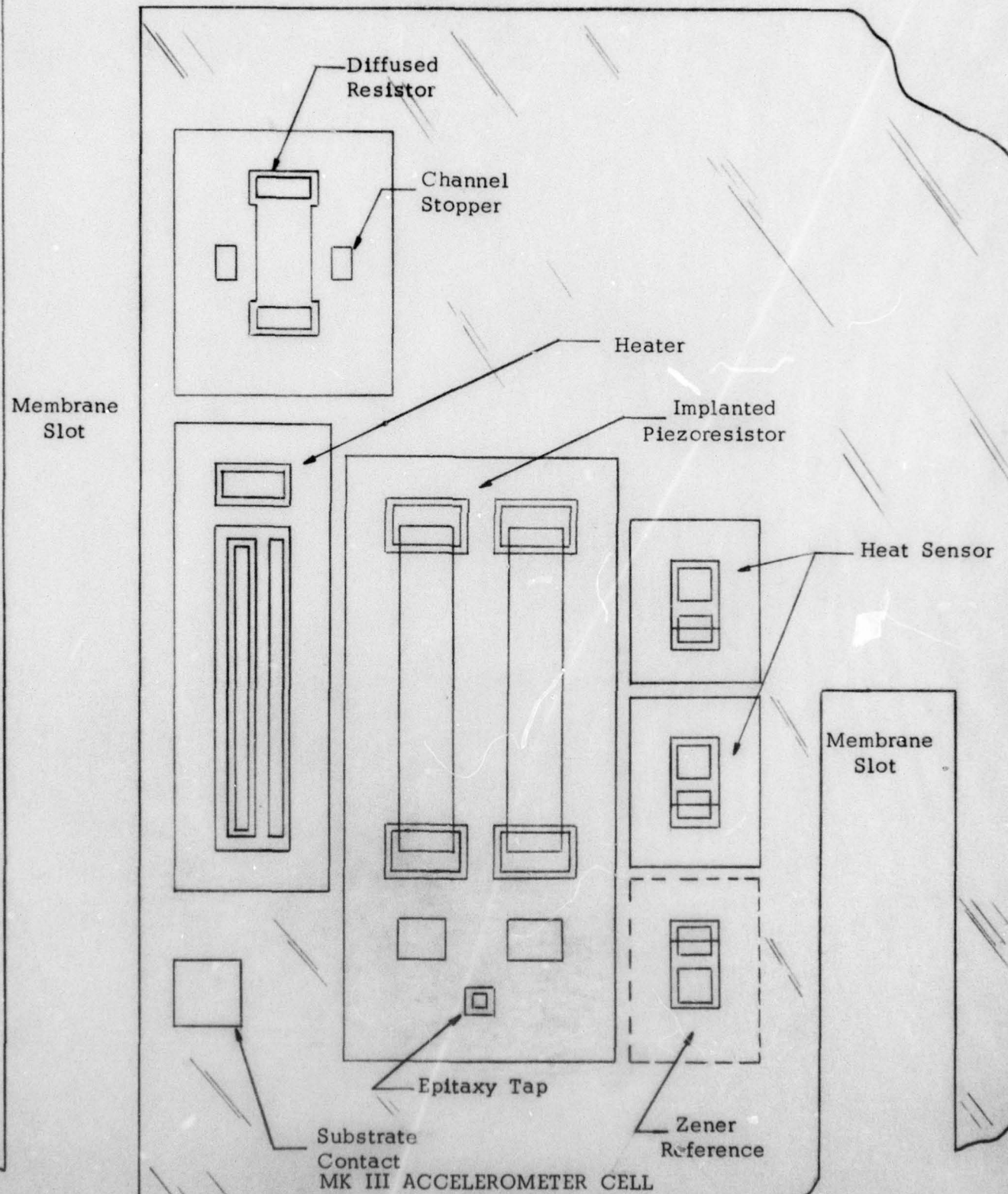


Fig. 35



MK III ACCELEROMETER CELL

Fig. 36

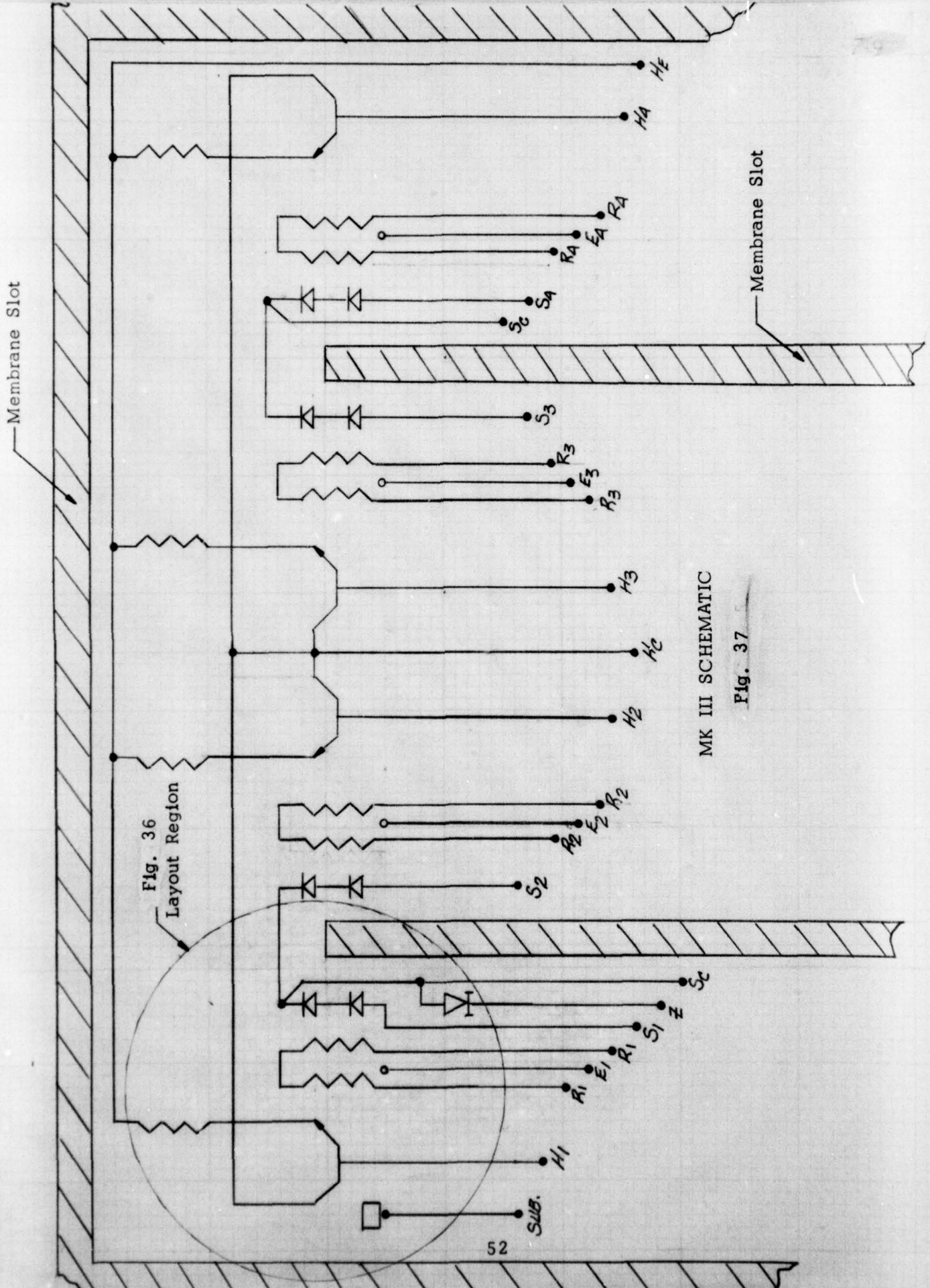


Fig. 36
Layout Region

MK III SCHEMATIC

Fig. 37

Membrane Slot

Membrane Slot

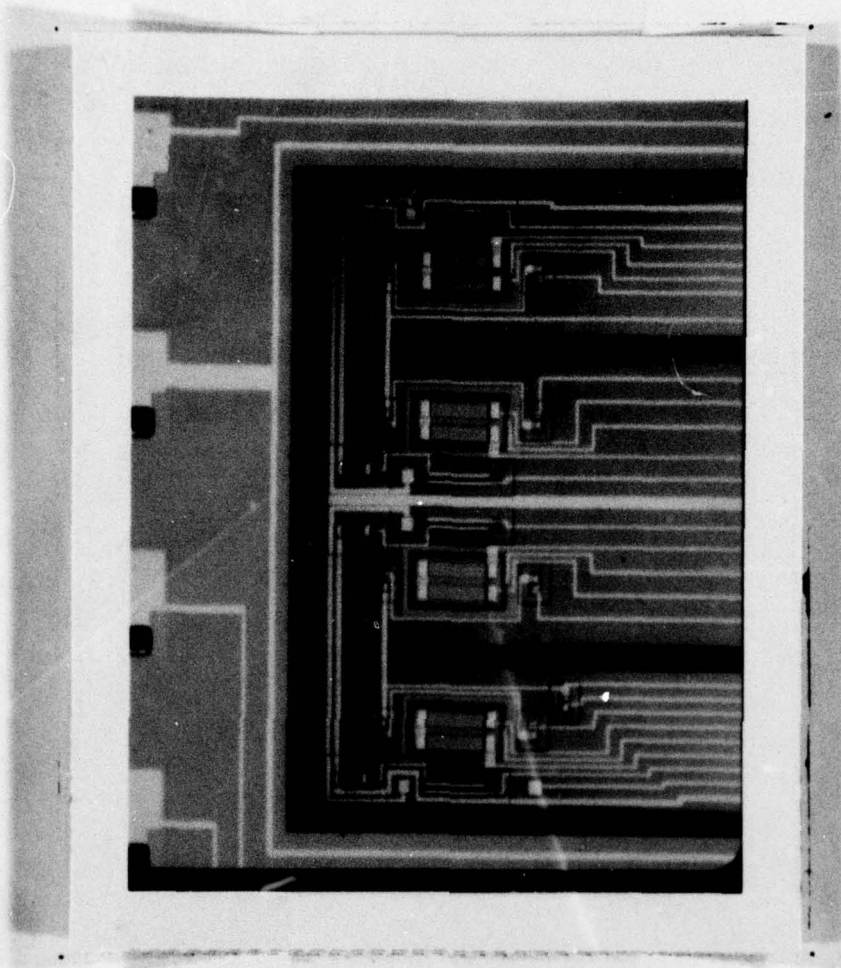


Fig. 38

Piezoresistor/Temp. Control Active Region

The geometric relationship of the piezoresistors with the heater-sensor circuitry is shown in this photo. Note the exact symmetry of the geometries as they relate to the membrane slots.

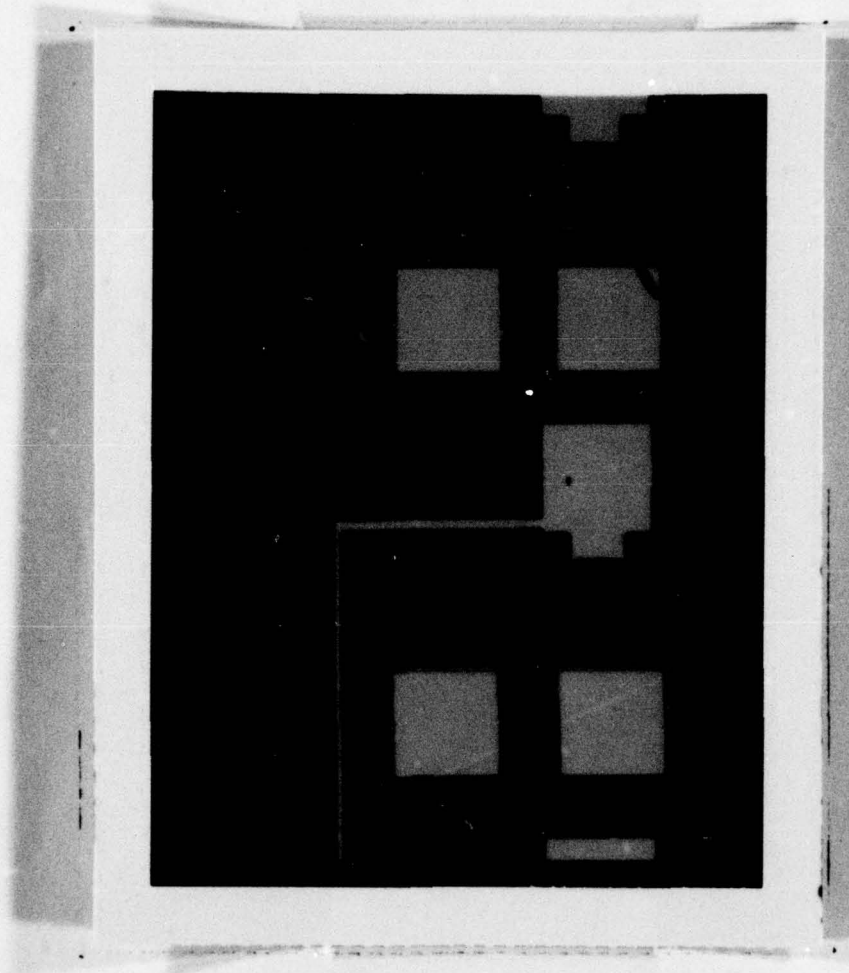


Fig. 39

Resistor Test Structures

These test resistors are used as "in process" controls for monitoring the exact values of the related active circuit resistors. The top resistor is diffused and typically has a 130 ohm/square value. The lower resistor is ion implanted to a 1000 ohm/square value.

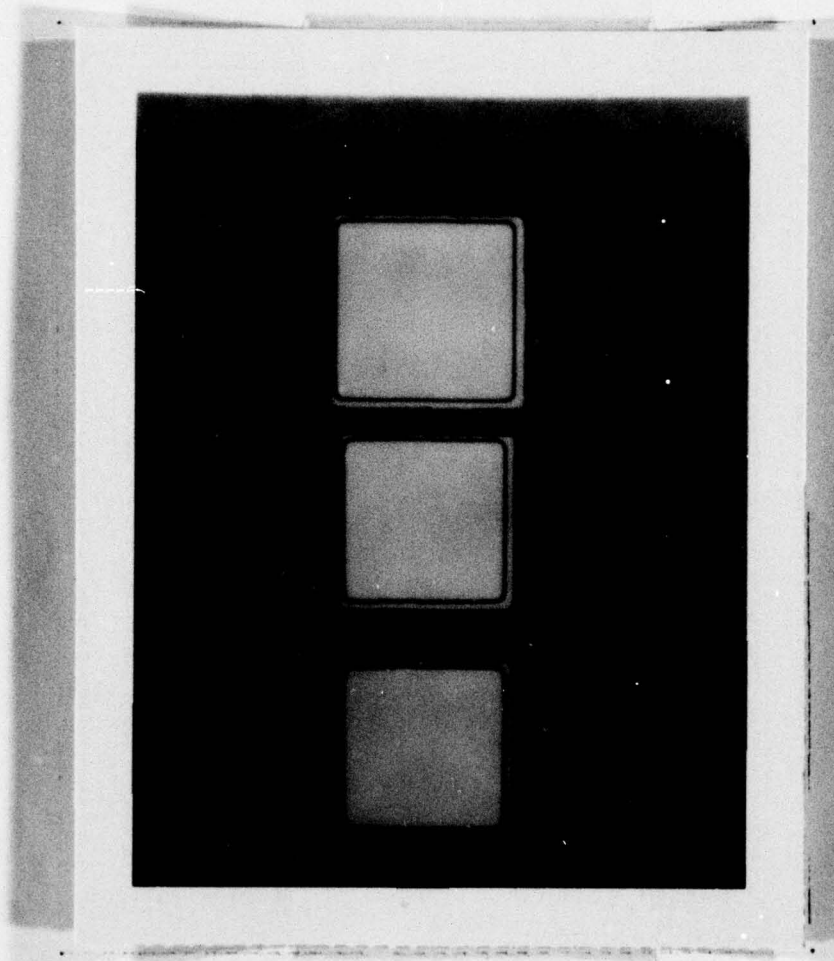


Fig. 40

Transistor Test Structure

This transistor is an enlarged structure which is easily accessed via probes for the analysis of electrical parameters such as current gain, and junction thresholds. The electrical results of this structure are representative of the much smaller active transistors and also provides an "in process" control.

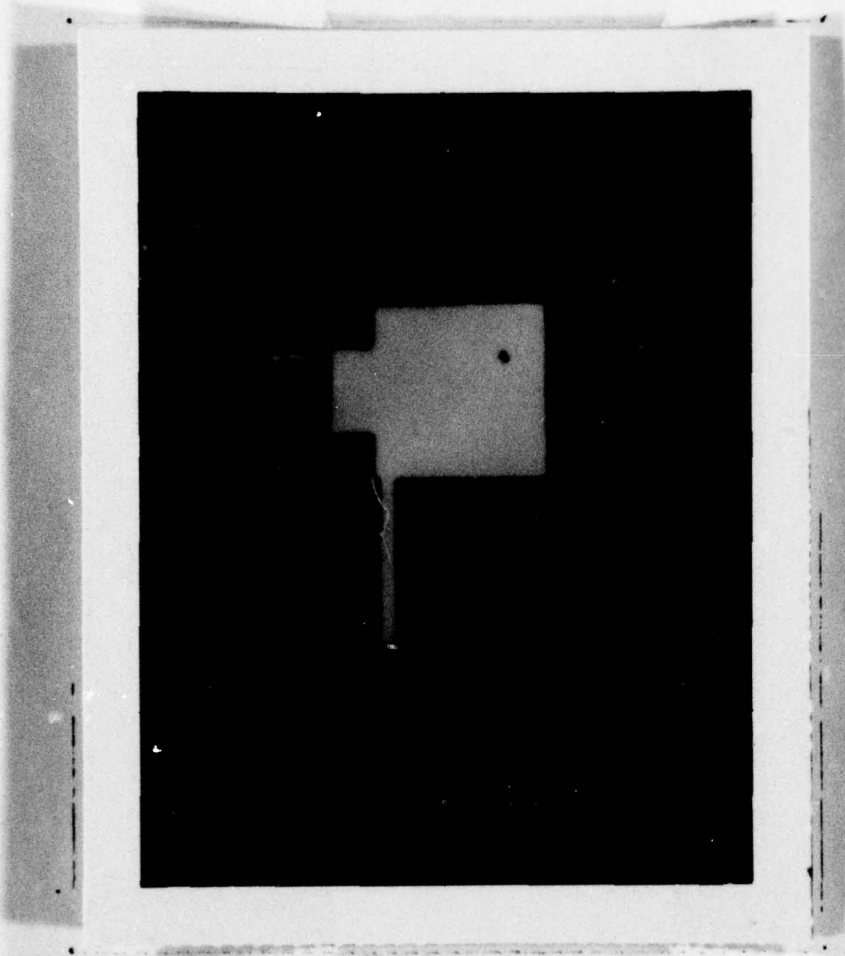


Fig. 41
Probing-Bonding Pad

The probing pad is made purposely large for easy probe access (note probe mark). The gold pillar is the solder bonding pad. This, as shown, is electrically continuous with the probing pad. This configuration is necessary because if the electrical probing were done on the bonding pad, it would deform due to mechanical pressure and make bonding difficult because of non-planarities.

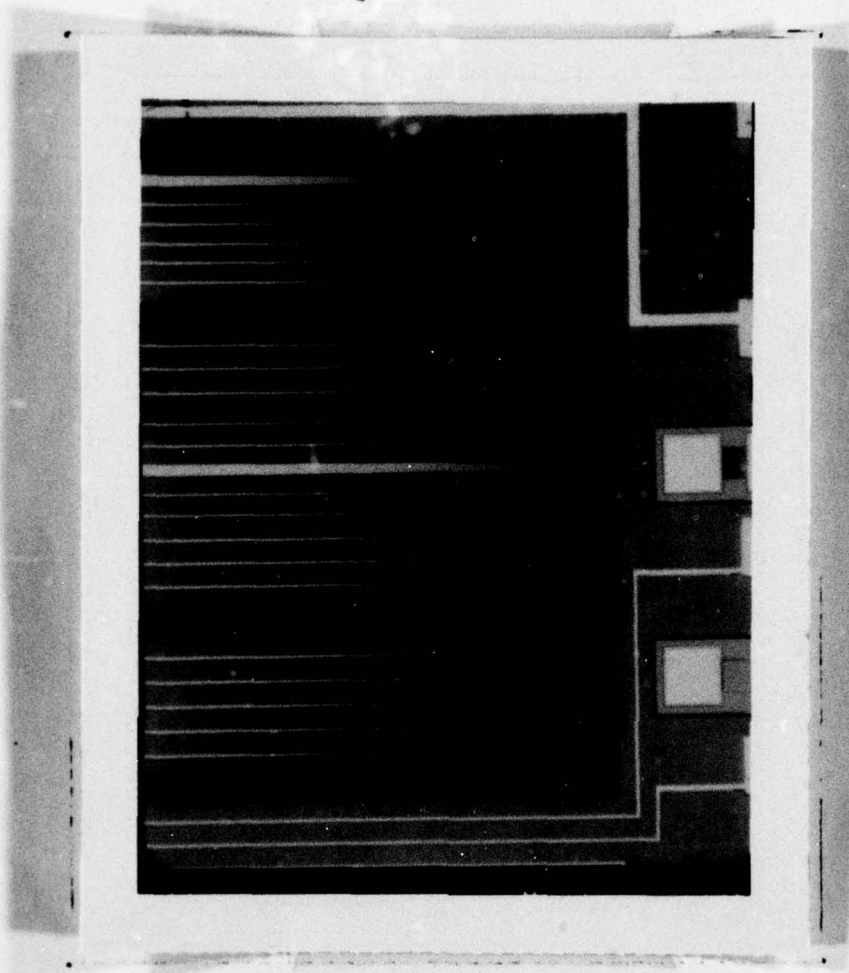


Fig. 42

Depth Gauges - Front Side

This row of slots represents an incremental 5μ progression in depth of $15 \mu\text{m}$ to $40 \mu\text{m}$ from top to bottom. These gauges are precisely formed during the membrane slot etch operation.



Fig. 43

Depth Gauges - Back Side

The final membrane thickness can be precisely controlled to a variety of desired thicknesses by observing the emergence of the depth gauge progression and terminating the etching process when the desired depth gauge appears. In this photo all but the 15 μm depth gauge have appeared; therefore the membrane thickness is between 15 and 20 μm . The actual thickness can be mathematically determined by measuring the width of the smallest opening and applying a trigonometric formula.

MK III SENSOR EVALUATION

Five fabrication variations were manipulated in the latest run of Mk III accelerometers, in order to gain some important comparative information. The factors varied were the type of piezoresistor and the method of sensor mounting. These are summarized in the table below:

<u>Variation</u>	<u>Description</u>
A	Ion-implanted piezoresistors with integral heater/sensors, mounted on interface chip
B	Same as A, except sensor was not mounted on Interface Chip
C	Ion-implanted piezoresistors only, no Interface Chip mounting
D	Same as C, except with Interface mounting
E	Diffused piezoresistors only, no Interface Chip mounting

The above variations were subjected to a five part evaluation for:

- 1) Sensitivity
- 2) Static Non-linearity
- 3) Noise
- 4) Temperature coefficient of bias
- 5) Damping

The measurement techniques used for all of these tests have been previously described and will not be discussed here. The test results which consider only the sensor bridge with 10 volts excitation, no amplification, and no temperature control, appear in the following table.

Fig. 44

	Sensitivity $\frac{\Delta R}{R}$ and V/g	Static Non-linearity	Noise Vpp 1Hz NBW	Tempco $\frac{\Delta V}{\Delta T}$	Damping Q Factor
A	124 ppm/g 1.24 mV/g	.20%	8 μ V	50 μ V/C°	15
B	142 ppm/g 1.42 mV/g	.10%	10 μ V	220 μ V/C°	>250
C	148 ppm/g 1.42 mV/g	.10%	6 μ V	120 μ V/C°	>250
D	133 ppm/g 1.33 mV/g	.15%	6 μ V	150 μ V/C°	15
E	190 ppm/g 1.98 mV/g	.30%	7 μ V	110 μ V/C°	>250

Some general conclusions can be drawn from the summary table. First, the sensitivity of all the ion-implanted units is much lower than the diffused unit, and in addition, much lower than previous runs of the Mk II transducer. It is believed that the sensitivity reduction is due to attenuation of the implant dopant in the SiO₂ layer. Thinning the oxide will reduce the attenuation effect and should increase the doping and sensitivity factor. Second, the temperature coefficient of the bridge (tempco matching) does not show any dramatic correlation with either the piezoresistor type or the mounting technique. This is an unexpected result and will have to be studied further. In general, the tempco of the Mk III units are better than the Mk II's; however, the tempco coefficient is still too large in relation to the bridge sensitivity to acceleration. Third, the non-linearity of the ion-implanted units is substantially less than the non-linearity of the diffused unit. This is also a new and surprising result, which does not correlate with previous runs of diffused piezoresistor units. Fourth, the noise in the bridge output is slightly higher for the A and B units over the other variations. This is probably due to stress effects introduced by the buried layer, and other processing steps required to make the heaters and sensors. And last, the damping Q shows a normal variation with mounting technique. The Q of the Interface mounted units correlates well with previous measurements on Mk II devices.

Two other factors were observed in the evaluation of these Mk III units. All the transducers tested suffered from a parasitic resistance problem due to very thin metal on the chip. This was exceptionally bad for the Interface mounted units which showed parasitic resistances of 1K or more. It had a drastic effect on resistor matching, noise, and evaluation of the thermal control loop. Additional runs are being tried to eliminate this problem, which was not observable previously on the Mk II Interface assemblies. The other factor that was observed was an unusually high "misalignment" error on the static linearity runs. This error, which used to be less than a degree for Mk II units, is running typically 20 to 50 degrees on the Mk IIIs. We have no logical explanation for this observed phenomenon, but realize from the dynamic testing at Stanford University, that we must find the origin of this problem.

The quad temperature control loop was evaluated with full Mk III units mounted on interface chips. Although the individual temperature control loops worked as expected, the overall system did not work properly due to mismatched components in each control loop and cross coupling between loops. We had transferred the problem of matching piezoresistors, to matching of heaters and sensors, which turned out to be just as difficult. In addition, since the temperature control system stabilized the chip at a temperature far above ambient, the bridge output became noisy and experienced large drifts due to the higher leakage currents at these temperatures. The temperature performance was actually better with the control loops disconnected.

MK III TESTING
AT
STANFORD UNIVERSITY

The conventional method for testing nonlinearities in an accelerometer is to use a precision dividing head. In some unusual instances, centrifuge measurements to enhance coefficients which are too small to evaluate accurately on the dividing head may be used. We had chosen to use a combination of dividing head and sinusoidal excitation. The sinusoidal excitation, we felt, would give us two types of information. The first would be an indication of nonlinearities, and the second, a better understanding of the dynamic characteristics of the instrument. It has developed that there are phenomena we don't fully understand appearing in the data in the side of the way of excitation. For complete understanding of the instrument, this is fortuitous because whatever these phenomena are, it is best that they be fully understood before the instrument is used in the field. Until this is understood, it will not be possible to infer nonlinearities from the vibration test and we must limit ourselves to use of the dividing head information.

The dividing head tests have been very encouraging to date. A difference signal, as well as the output of the Signetics device and the reference accelerometer, a Bell model 7, are each available. Tests performed last Fall and repeated this week indicate good sine wave characteristics for each instrument. We have therefore concentrated on the difference signal in evaluating the performance of the Signetics instrument. The Bell model 7 should be linear at least to a part in 10^4 in this environment and we are discussing the following data on the basis that the Bell serves as a fundamental standard.

The tests performed include an identification of the direction of the sensitive axis for each instrument. After both instruments were mounted

on the dividing head and a bias correction made for the Signetics instrument, zero readings were taken for each instrument. These occur in two locations as long as the bias is smaller than the peak reading of the instrument. The average of these two readings correspond to the sensitive axis up or down. By adding 90 degrees, the sensitive axis is horizontal. At that orientation the output reading of the instrument is its bias. This was performed for each instrument. The data are given in Fig. 45.

The difference in the sensitive axes of the two instruments was 56'30". No attempts was made to zero this relative orientation. Rather, the fitting of the difference signal was done. Two runs were made—one with very accurately determined angles which took up 15 mins to complete, and then a repeat was performed which was done in less than 5 mins. The data and the plotted values are shown in Figs. 46 and 47. The thermal drift, due to the fact that the temperature compensation that is being developed for the Signetic instrument was not being used at this time is evident in the data. Allowing for this and a bias, one can estimate the expected sinusoidal component which should be a cosine function of the different signal assuming that the scale factor was appropriately matched. The fit is within the accuracy of the measurements, leaving residuals, which are on the order of 0.1 %.

We conclude, on the basis of these data that the Signetics instrument is probably linear to 0.1%. From the sinusoidal test, however, we have observed an apparent phase shift in the sine wave outputs which seems almost independent of frequency. This amounts to between $1\frac{1}{2}$ deg to $2\frac{1}{2}$ deg in the range of 15 to 150 Hz. No normal phase shifting circuitry can explain this small change in phase over a decade of frequencies. We therefore assume that there is a mechanism for producing an out-of-phase component in the silicon material due to a perhaps misaligned sensitive axis of the instrument. This mechanism is not understood at the present time. The latest Mark III exhibits a larger misalignment and therefore should provide us with a more sensitive way of determining what this mechanism is.

We are very encouraged by the dividing head tests performed to date. We do not feel that the lack of understanding of the sinusoidal test is unusual for this stage of development for a new instrument type. We therefore continue to feel this is a promising instrument which deserves continued

evaluation. It is our hope that the added understanding the additional tests will provide us will indicate clearly whether or not there is a simple fix or relatively straightforward compensation possible, or whether there are intrinsic difficulties in the approach.

We must next perform the most likely tests to help us understand why there appears to be a frequency independent relative phase in the difference signal of the accelerometers when we shake them. Using identical device, e.g., the Mark II, should clearly show whether this effect is due to instrumentation or not. the Mark III appears to have a larger phase angle so two of these devices may provide the most insight.

Fig. 45

THREE POINT ZERO PHASE AND BIAS DETERMINATION

(° = deg; ' = arcminute; " = arcsecond)

Comment	Bell	Signetics
zero readings	60° 10' 28" and 239° 30' 10"	60° 1' 19" and 327° 46' 20"
expected maximum	149° 50' 19"	148° 53' 49"
reading at expected maximum	-182.0 mV	+233.8 mV
with respect to expected maximum:		
+10°	-179.2 mV	+229.8 mV
-10°	-179.2 mV	+229.7 mV
90° from expected maximum (= bias)	59° 50' 19" 1.074 mV	58° 53' 49" -5.3 mV
difference in sensitive axis directions	(149° 50' 19") - 56' 30" - (148° 53' 49")	

Fig. 46

FIRST RUN

ED Least Squares Fit Sine
Leitz DATA

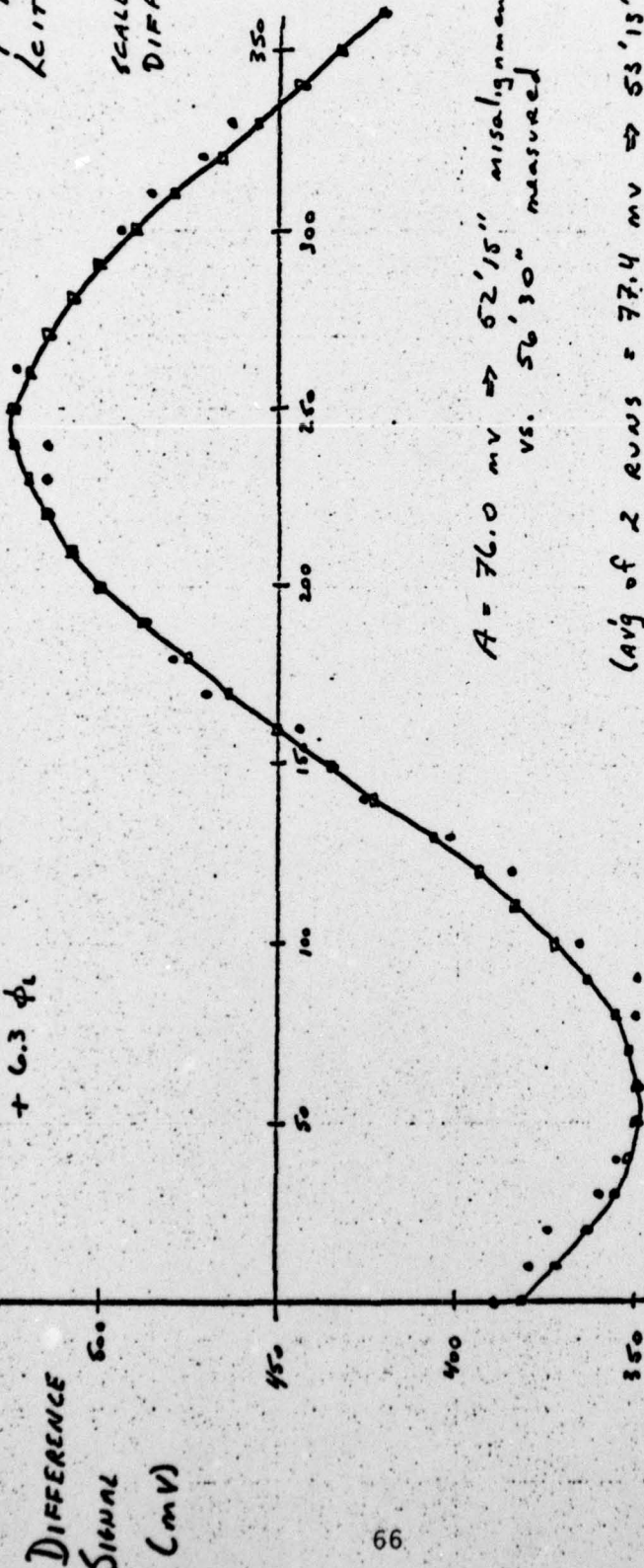
$$SINE = 419 \sin 76.0 \text{ SW} (\phi_2 + 130^\circ) + 6.3 \phi_1$$

DATA TAKEN:

R DEBON, E. NESO
3/7/77

LEITZ DIVIDING
HEAD

SCALE FACTOR OF
DIFFERENCE SIG.
= 5 VOLTS/9



$A = 76.0 \text{ mV} \Rightarrow 52'15''$ misalignment
vs. $56'30''$ measured

(AVG of 2 RUNS = $77.4 \text{ mV} \Rightarrow 53'13''$ misalignment)



NOTE
CHANGE
of
scale

$$\text{MEAN} = 2.54 \times 10^{-5}$$

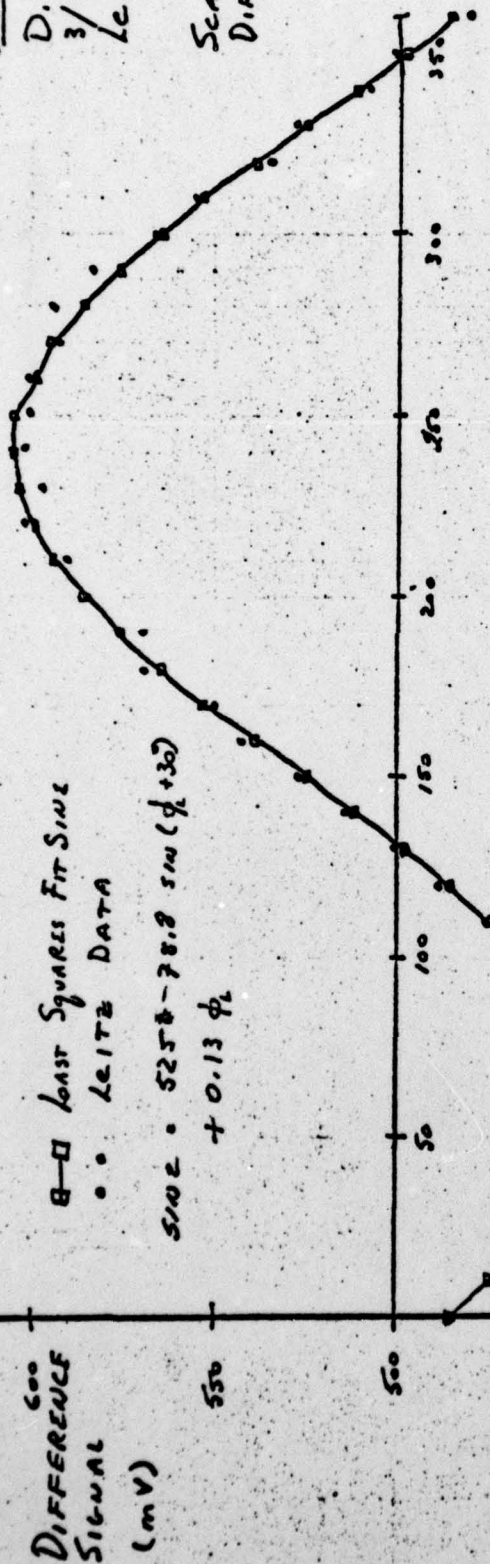
$$16 \cdot 5.35 = 0.11\%$$

Second Run

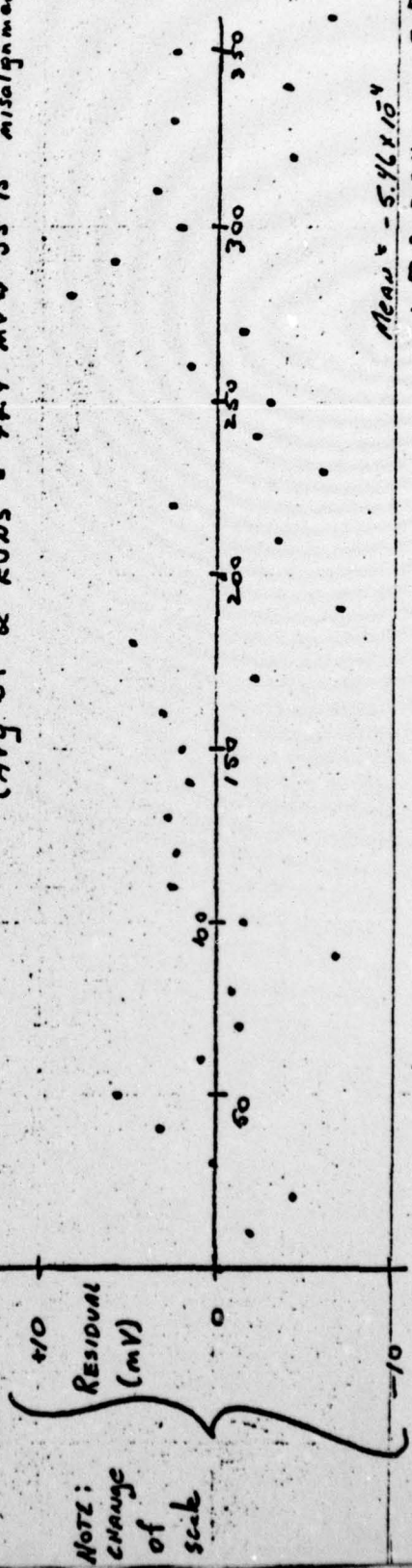
Fig. 47

DATA TAKEN
 D. Debra, E. Mc
 3/7/77
 LEITZ DIVIDING
 HEAD
 SCALE FACTOR
 DIFFERENCE SIG
 $5 \frac{\text{VOLTS}}{g}$

—□— LEAST SQUARES FIT SINE
 .. LEITZ DATA
 SINE = $525\theta - 78.8 \sin(\theta + 30)$
 + 0.13 ϕ



$A = 78.8 \text{ mV} \Rightarrow 54'11''$ MISALIGNMENT
 VS. $56'30''$ MEASURED
 (Avg of 2 RUNS = $72.4 \text{ mV} \Rightarrow 53'13''$ misalignment)



MEAN $\sigma = 5.46 \times 10^{-4}$
 $1 \sigma = 3.74 = 0.07 \%$

NOTE:
 CHANGE
 OF
 SCALE

CRITIQUE AND RECOMMENDATIONS

There are two basic problems with the current Mk III accelerometer. One is the misalignment error that was introduced by going to the Mk III resistor orientation. We have done additional experiments to show that the parallel resistor arrangement can be made to give low alignment errors, if opposite resistor pairs from both ends of the membrane are used. We were able to reduce the error on any given device from 20 degrees to less than 2 degrees by this method. Additional work will have to be done in future work to verify if this method yields both lower temperature coefficients and low alignment errors.

The last problem with the Mk III is the inability to achieve critical damping with the interface/squeeze film technique. Fluid damping seems like the next best method to try, but an extensive study on damping material compatibility with silicon circuits will have to be made.

The stress sensitivity, non-linearity and the excess noise, of the Mk III accelerometer is marginally usable, but really needs to be improved. The sensitivity could be improved by accommodating larger proof masses or by thinning the membrane of the device. The non-linearity of our device is good, but it does deteriorate on certain fabrication runs, and needs to be controlled more accurately. Finally, the excess noise is slightly high for silicon resistors and could be improved by cleaner processing techniques.

We have made numerous design innovations since the Mk I, to attempt to reduce the temperature sensitivity of our piezoresistive sensor. Other than the change made in the Mk III series (parallel vs. orthogonal resistors), nothing has seemed to reduce the overall temperature problem to any great extent. The remaining courses of action must take one of three paths. The first path is to remain with the present folded cantilever design with silicon piezoresistors and

- a) do a complete three dimensional stress analysis on the membrane structure, and
- b) investigate improved methods of photolithography for resistor matching.

The second path is to do all of the above, except try to find a substitute material for the piezoresistors that will have better sensitivity to stress and lower temperature coefficients. The third path is to abandon the folded cantilever structure entirely and start a totally new design based on a more conventional beam cantilever concept. For this third path, silicon piezoresistors might be used since the unit could be stressed more for a given acceleration (larger proof mass). Future work on a silicon accelerometer must be guided along one or more of these three paths.

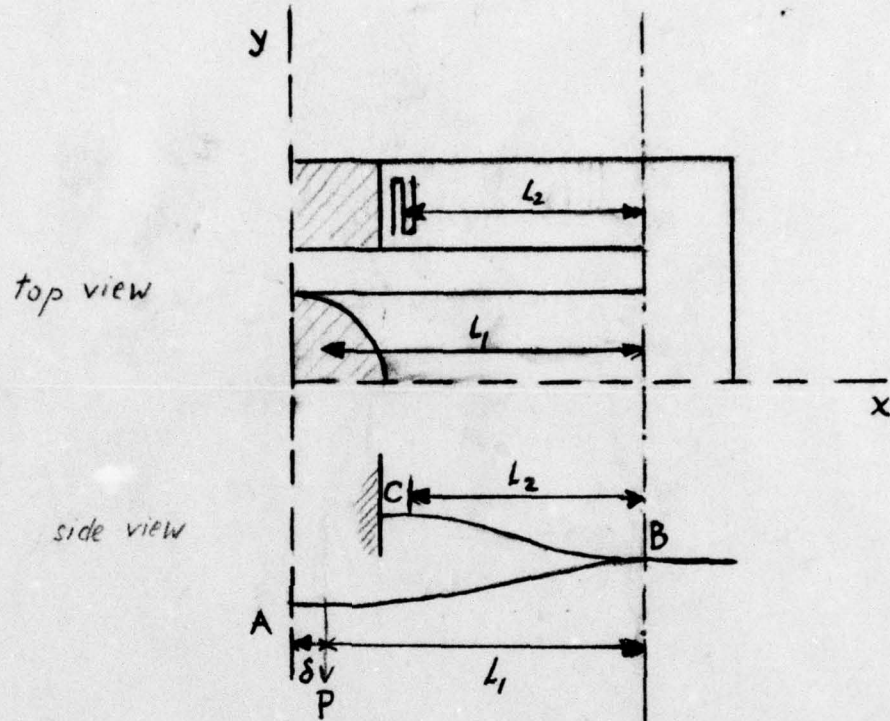
APPENDIX

- A. Theory of the Piezoresistive Sensor
- B. Temperature Analysis of Membrane

APPENDIX

Theory of the piezoresistance sensor

A. Mechanical Problem



Symmetry axes x and y allow the problem to be divided into four identical problems.

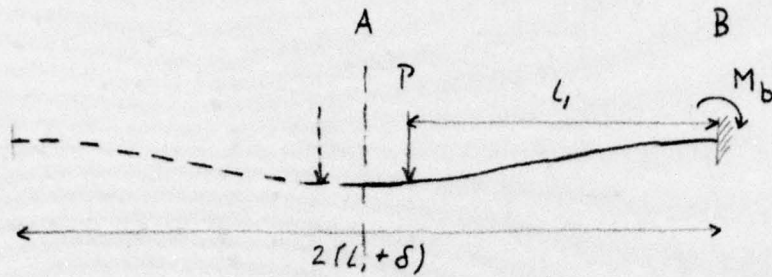
Boundary conditions

Point A: Because of symmetry the beam is horizontal at Point A. The distributed external forces are reduced to an equivalent force $P = \frac{m}{4} a$ where $a =$ acceleration, $m =$ total mass.

Point B: We assume a stiff plate such that the beam enters at zero angle.

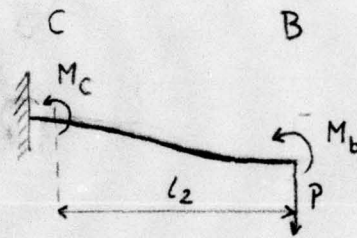
Point C: The beam is built in and therefore enters at zero angle.

The whole problem is statically indeterminate. But if we assume that the horizontal components of the force are zero, we can divide the problem into 2 determinate problems.



The result is $M_b = 2 Pl_1 \frac{l_1 + 2\delta}{4(l_1 + \delta)}$

$$\lim_{\delta \rightarrow 0} M_b = \frac{Pl_1}{2}$$



In point C the resultants are P and

$$M_c = -M_b + Pl_2$$

The resultant couple in point C is therefore

$$M_c = P \left(-\frac{l_1}{2} + l_2 \right)$$

Using the first approximation, the maximum stress at the beam surface becomes

$$\sigma_m = \frac{h M_c}{I}$$

where $h = 1/2$ beam thickness

$$I = \frac{2}{3} bh^3$$

$b =$ beam width

The shear stresses are zero at the beam surface. The maximum stress is a linear function of the applied force only if the changes in l_1 and l_2 are infinitesimal. To approximate the error, we assume that the sum

$$y_1^2 + l_1^2 = \text{constant} = l_{10}^2$$

where

$$y_1 = \left[\frac{P l_{10}^3}{12EI} \right] \times 2$$

is the vertical deflection of the beam (in first approximation) that extends from point A to B.

The change in stress is therefore caused by a nonlinear factor of

$$\frac{l_{10}^{-1} l_1}{l_{10}} = \frac{1}{2} \left(\frac{y_1}{l_{10}} \right)^2$$

which has to be less than the required nonlinearity. This calculation replaces the shape of the beam by a straight line and is therefore optimistic. A similar calculation is obtained for the beam between points B and C.

Example: $a = 1g \approx 10^3 \frac{\text{dyne}}{\text{gr}}$ $m = 10^{-2} \text{ gr}$
 $b = 5 \times 10^{-2} \text{ cm}$ $h = 1.25 \times 10^{-3} \text{ cm}$
 $E = 1.66 \times 10^{12} \frac{\text{dyne}}{\text{cm}^2}$ $\delta = 0.016 \text{ cm}$
 $l_{10} = 0.160 \text{ cm}$ $l_{20} = 0.103 \text{ cm}$

The results $P = 2.5 \text{ dyne}$ $I = 6.5 \times 10^{-11} \text{ cm}^4$
 $M_{co} = 2.5 (-0.080 + 0.103) = 5.8 \times 10^{-2} \text{ erg}$

$$\sigma_m = \frac{1.25 \times 10^{-3} \times 5.8 \times 10^{-2}}{6.5 \times 10^{-11}} = 1.12 \times 10^6 \frac{\text{dyne}}{\text{cm}^2}$$

$$y_1 \approx \frac{2.5 \times (0.16)^4}{24 \times 1.66 \times 10^{12} \times 6.5 \times 10^{-11}} = .79 \times 10^{-4} \text{ cm}$$

$$\frac{1}{2} \left(\frac{y_1}{l_{10}} \right)^2 = \frac{1}{2} \left(\frac{6.3 \times 10^{-7}}{1.6 \times 10^{-1}} \right)^2 = \frac{1.59 \times 10^{-7}}{1.59 \times 10^5} \text{ at } 1g$$

at 10g

With this arrangement a displacement that results in breakage of the crystal ($\sigma_m = 10^{10}$ dyne/cm²) would still only result in a nonlinearity of the order of $(I_0 - 1)/I_0 < 10^{-3}$. It can be shown that the distributed forces do not change the linearity.

B. Piezoresistance Bridge

In order to measure the stress the piezoresistance effect is used. The resistors are diffused p-type layers with surface concentrations of the order of 10^{18} cm⁻³ oriented parallel to the [110] directions. Resistors are either parallel (longitudinal resistors) or orthogonal (transversal resistors) to the direction of the stress. The resulting changes in resistance become:

$$\frac{\Delta R_l}{R_l} = \frac{\pi_{11} + \pi_{12} + \pi_{44}}{2} \sigma_m = \pi_l \sigma_m$$

$$\frac{\Delta R_t}{R_t} = \frac{\pi_{11} + \pi_{12} - \pi_{44}}{2} \sigma_m = \pi_t \sigma_m.$$

Typical values for π_l and π_t at 300°K would be

$$\pi_l = 72 \times 10^{-12} \frac{\text{cm}^2}{\text{dyne}}$$

$$\pi_t = -66 \times 10^{-12} \frac{\text{cm}^2}{\text{dyne}} .$$

These resistors can be arranged in a bridge of which the sensitivity $\Delta V/2V_0$ shall be determined.

$$\frac{\Delta V}{2V_0} = \frac{V_1 - V_2}{2V_0} = \frac{1}{2} \frac{\frac{\Delta R_1}{R_1} - \frac{\Delta R_t}{R_t}}{1 + \frac{1}{2} \left(\frac{\Delta R_1}{R_1} + \frac{\Delta R_t}{R_t} \right)}$$

Using our example with $\sigma_m = 1.12 \times 10^6 \frac{\text{dyne}}{\text{cm}^2}$ the sensitivity for a displacement of $1 \mu\text{M}$ becomes:

$$\frac{\Delta V}{2V_0} = 0.78 \times 10^{-4}$$

and the nonlinearity in the denominator

$$\frac{1}{2} \left(\frac{\Delta R_1}{R_1} + \frac{\Delta R_t}{R_t} \right) = 3.4 \times 10^{-6} \ll 1.$$

Conclusion:

From the foregoing calculations it can be concluded that the linearity of the transducer is not limited by the structure of the beam, but by the accuracy of the bridge for stresses up to the breakstress. The ratio of the nonlinearity of the bridge to the sensitivity of the bridge is a constant given by $(\pi_1 + \pi_t)/(\pi_1 - \pi_t) = 4.4 \times 10^{-2}$ in our example. Thus a sensitivity of 2% would result in a nonlinearity of $< 0.1\%$. The nonlinearity of the piezoeffect has not been considered since it cannot be derived theoretically and has to be measured. From present evidence the effect is linear as long as Hooke's law is obeyed and the crystal is free of defects.

TEMPERATURE ANALYSIS OF MEMBRANE

Find the thermal resistance of a plate with area A and thickness t that is suspended in air above an infinite thermal sink.

A. Solution based on conductivity of air

$$\text{heat flow (watts)} = \frac{A k_m}{l} T$$

T = difference in temperature
 k_m = conductivity constant
 A = area
 l = path length

$$k_m \text{ for air} = \frac{.165}{2903} \times 4.1868 = 2.3796 \times 10^{-4} \frac{\text{watt}}{\text{C}^\circ \text{cm}} ;$$

therefore,

$$\text{thermal resistance} = \frac{T}{\text{heat flow}} = \frac{l}{A k_m}$$

for a spacing of 10 mils = .1254 cm, and

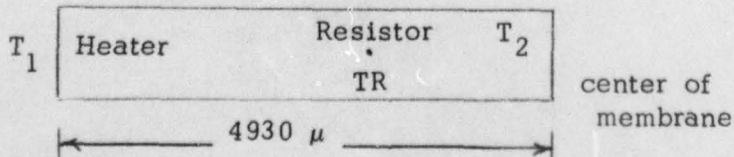
$$\text{Area} = 8.8689 \times 10^6 \mu^2 = 0.88689 \text{ cm}^2$$

$$\text{thermal resistance} = \frac{.0254 \text{ cm}}{(.088689 \text{ cm}^2)(2.3796 \times 10^{-4})}$$

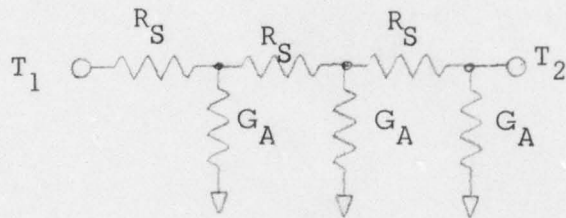
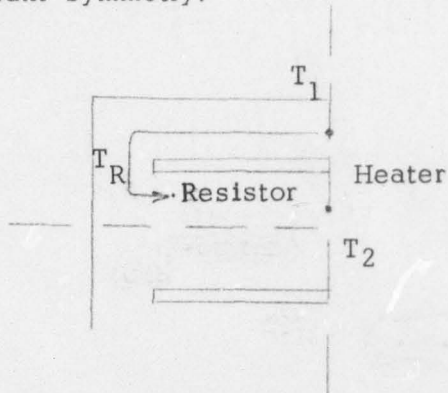
$$\Theta_{\text{cond}} = 1203 \text{ }^\circ\text{C/W}$$

This thermal resistance is significant with respect to the sheet thermal resistance of the membrane ($400^\circ\text{C/W}/\square$).

Now model actual situation as a continuous loss transmission line for temperature.



This is a "linearized" version of the actual geometric form, using 4 quadrant symmetry.



R_S is the silicon sheet thermal resistance.

G_A is the conduction loss from the membrane to ambient through air.

The above resistor circuit is easily modeled as a transmission line with $L = C = 0$.

$$Z_o \text{ of transmission line} = \frac{R_e}{G_e}$$

$$\alpha \text{ loss coefficient of line} = R_e G_e$$

where R and G are resistance and conductance per unit path length.

The transmission line equations for this situation are

$$T_1 = \frac{T_2}{2} [e^{\alpha l} + e^{-\alpha l}]$$

$$P_1 = \frac{T_2}{Z_o} [e^{\alpha l} - e^{-\alpha l}]$$

T_1 = temperature at the sensor

P_1 = 1/4 of total heater power injected into membrane

T_2 = temperature at center of membrane

The transmission line equations assume an "open circuit" at T_2 , i.e. no power transfer at the center of the membrane. This is equivalent to $Z_{LOAD} = \infty$ in normal lines.

Determination of R and G, α and Z_o

$$K = 1.2 \frac{W}{C^\circ \text{cm}}$$

$$R_\rho = \frac{1}{K} \frac{1}{ty}$$

$$= \frac{1}{1.2} \frac{C^\circ \text{cm}}{W} \times \frac{1}{(25 \times 10^{-4})(500 \times 10^{-4})}$$

$$R_\rho = 6666 \frac{^\circ\text{C}}{W \text{ cm}}$$

$$G_\rho = \frac{K(y)}{S}$$

$$= 2.379 \times 10^{-4} \frac{W}{C^\circ \text{cm}} \frac{500 \times 10^{-4} \text{ cm}}{.0254 \text{ cm}}$$

$$G_\rho = 4.683 \times 10^{-4} \frac{W}{C^\circ \text{cm}}$$

$$Z_o = \sqrt{\frac{R_\rho}{G_\rho}} = \sqrt{\frac{6666}{4.683 \times 10^{-4}}} = 3772$$

$$\alpha = \sqrt{R_\rho G_\rho} = \sqrt{6666 (4.683 \times 10^{-4})} = 1.766$$

Evaluation of Transmission Line Equations

$$T_1 = \frac{T_2}{2} \left[e^{\alpha l} + e^{-\alpha l} \right]$$

$$P_1 = \frac{T_2}{Z_o} \left[e^{\alpha l} - e^{-\alpha l} \right]$$

for $l = 4930 \mu$

and $\alpha = 1.766$, $Z_o = 3772$

$$T_1 = 1.403 T_2$$

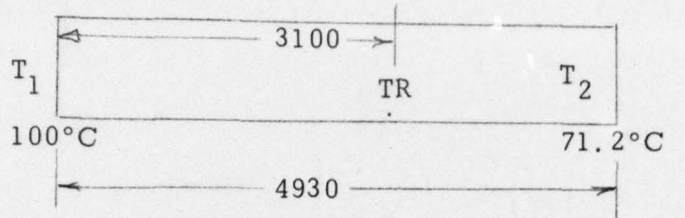
$$P_1 = 5.222 \times 10^{-4} T_2$$

- for a temperature rise at T_1 of 100°C

$$T_2 = 71.2^\circ\text{C}$$

$$P_1 = 37.2 \text{ mW}$$

A similar technique is used to find T_R , the temperature at the resistors.

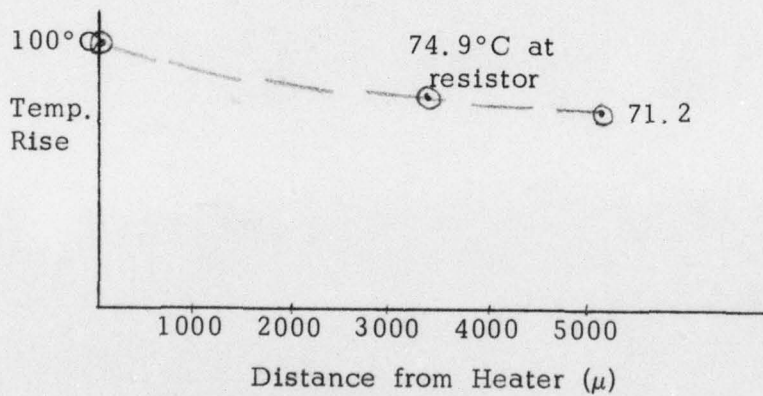


$$T_R = \frac{T_1}{2} \left[e^{\alpha(4930-3100)} + e^{-\alpha(4930-3100)} \right]$$

$$T_R = \frac{100}{2} [1.3815 + .7238]$$

$$T_R = 1.05 T_2$$

$$T_R = 74.9^\circ\text{C}$$



Additional Heat Losses from Radiation and Natural Convection

B. Thermal resistance based on radiation

$$\text{heat rate} = \epsilon 3.68 [T_o^4 - T_a^4] \times 10^{-11} \text{ watts/in}^2$$

$$\begin{aligned} \text{heat} &= (.5)(3.68) [40.0^4 - 300^4] \times 10^{-11} \\ &= .322 \text{ watts/in}^2 \times \frac{\text{in}^2}{(2.54)^2 \text{ cm}^2} \end{aligned}$$

$$\text{heat rate} = .0499 \text{ watts/cm}^2$$

$$\Theta_{\text{rad}} = \frac{100^\circ\text{C}}{.0499 \times (.0886 \text{ cm}^2)} = 22614 \text{ }^\circ\text{C/W}$$

C. Thermal resistance based on natural convection

$$\begin{aligned}\text{heat rate} &= 11.70 (T)^{1.25} \times 10^{-4} \\ &= .3699 \text{ watts/in}^2 = .0573 \frac{\text{w}}{\text{cm}^2} \\ \Theta_{\text{conv.}} &= \frac{100^\circ\text{C}}{.0573 \frac{\text{w}}{\text{cm}^2} (.0886 \text{ cm}^2)} = 19681 \text{ }^\circ\text{C/W}\end{aligned}$$

∴ These are much higher than conduction!

Now find thermal resistance of membrane to interface chip, assuming 25 μ separation and conduction of heat through air.

$$\begin{aligned}\Theta_{\text{cond.}} &= \frac{l}{A km} \\ &= \frac{25 \times 10^{-4} \text{ cm}}{(.088689 \text{ cm}^2)(2.379 \times 10^{-4})} \\ \Theta_{\text{cond.}} &= 118 \text{ }^\circ\text{C/W}\end{aligned}$$

This is going to be troublesome, since there is also another conduction path through the bump pads. It means that it will be impossible to raise the temperature at the piezoresistors more than a few degrees. Therefore, control loop is useless!